

Direct Imaging of Radial Velocity Exoplanets

WFIRST-AFTA Coronagraph Study

12/18/2014

Aastha Acharya, aa533

Advisor: Dmitry Savransky, ds264

Contents

Abstract	2
Introduction	3
Literature Review	4
Exoplanet Background	4
Detection Methods.....	4
Radial Velocity Detection Method	7
Orbital Mechanics.....	10
Coronagraph Specification.....	11
Methodology.....	13
Results and Discussion.....	17
Conclusion.....	23
References	24
Appendix.....	26
Appendix A – Characteristics of visible exoplanets	26
Appendix B – Visibility time profiles for each exoplanet	27
Appendix C – Radial velocity and time range profiles for each exoplanet	31
Appendix D – contrast curve limitations for each exoplanet.....	35
Appendix E – Main code used for orbital modeling and simulation	39
Appendix F – Code used to gather all planetary information	42
Appendix G – Supplementary subfunctions.....	44
Appendix H – Code used for time range.....	45
Appendix I – Code used for contrast curve plotting.....	46
Appendix J – Code used to plot overall time distributions	47

Abstract

The study of exoplanetary systems is an accelerating field as we continue to discover new planets due to advances in detection techniques and instrumentation. However, the majority of planets are detected via indirect methods, such as radial velocity (RV) and transit photometry. These methods rely on observing the effects of exoplanets on the stars they are orbiting, and can therefore limit the planets we can detect and the information we can gather. To further expand the types of planets we can investigate, various direct imaging methods and tools are being developed. One such instrument is a proposed coronagraph for the Wide-Field Infrared Survey Telescope Astrophysics Focused Telescope Assets (WFIRST-AFTA). One science case for this instrument is the direct imaging and spectral characterization of previously discovered exoplanets.

In this work, we present a method to find the best times to directly image the subset of RV exoplanets detectable by WFIRST-AFTA. We model the orbits of RV exoplanets using their fit orbital parameters (and error ranges) along with unbiased priors for all unknown parameters. We then map the times (with respect to maximum elongation) when the exoplanet will be geometrically unobscured to the coronagraph to the corresponding radial velocity profiles in order to determine the best times for direct imaging. We find that only 22 out of 534 radial velocity exoplanets are detectable by coronagraph with an inner working angle (IWA) of 200 mas, and 68 using an IWA of 100 mas. These results are folded into a larger instrument model with other factors, such as the coronagraph contrast and throughput, also taken into consideration, to produce a more detailed prediction for the RV exoplanet imaging capabilities of the WFIRST-AFTA coronagraph.

Introduction

Exoplanets, also known as extrasolar planets, are planets outside of the solar system that orbit a different star. There are many motives behind studying these exoplanetary systems such as to gain better understanding of the formation of solar systems and in search of extraterrestrial life or, in the least, for a habitable environment that can potentially support life. The existence of these planets has been predicted for centuries, but the first certified discovery didn't occur until 1995 (Wolszczan, Frail). Since then, over 1849 exoplanets have been discovered using various detection techniques such as radial velocity, transit photometry, astrometry, timing, and microlensing (*The Exoplanet Handbook*, Introduction). Using these methods, orbital parameters associated with these exoplanets as well as their distance from Earth can be determined. However, most of these detection techniques are indirect and introduce many constraints which prevent us from further studying these exoplanets and discovering new ones.

Indirect methods of exoplanet discovery rely on observing the effects the exoplanets have on the stars they are orbiting, and can therefore limit the type of planets we can explore and the information we can gather. While possible, direct imaging method for detection of these exoplanets is rare and has many constraints. However, there are multiple advanced direct imaging instruments being developed that can improve this technique significantly and increase the number of exoplanets we can image. One such instrument is the Wide-Field Infrared Survey Telescope (WFIRST). We are particularly interested in the Astrophysics Focused Telescope Assets (AFTA) design of the telescope as it has a potential to include a coronagraph for exoplanetary studies. The coronagraph feature of the telescope will directly image and take spectra of a subset of exoplanets previously discovered using the radial velocity method as well as aid the search for new exoplanets.

The focus of this research will be in working with the given characteristics of the coronagraph and all the exoplanets previously detected by the radial velocity method to determine the most suitable times to directly image them. Orbits of the exoplanets can be simulated based on the given and/or estimated orbital parameters. Then, the radius of the projected orbit on to a viewer plane can be compared with the observable area radius based on the inner working angle of the coronagraph. This comparison can be used to draw conclusions about the visibility of the explanatory systems and the best times to directly image them. In turn, the derived conclusions will be used to further determine the best planets to image during a certain time range by projecting their radial velocity curves into the past and/or the future. Furthermore, contrast limitations of the instruments as well as the expected contrast of the planet will also be considered to further determine the visibility constraints and ultimately gather the best set of target exoplanets and corresponding times to directly image.

Literature Review

Exoplanet Background

There are many reasons why the search for exoplanets is considered important and top priority in the field of astronomy. As was mentioned previously, study of exoplanets can lead to extraterrestrial life, or at least help us find a habitable planet that can potentially support life in the future. Furthermore, learning more the exoplanetary systems can “help us understand our place in the universe.” (Harris, 2010) It can help us test our current understanding of the formation of solar and extrasolar systems. In addition, it will also provide insight into the formation of individual planets as well as the host stars, and perhaps even lead us to better understand our own solar system’s past and future. Hence, this topic has been given much interest currently and in the past.

The existence of exoplanets has been speculated for centuries with some of the early philosophers stating “there are infinite world both like and unlike this world of ours” (Epicurus, 324-270 BCE) and “in [this universe] are an infinity of worlds of the same kinds as our own” (Bruno, 1584). There were various searches being performed for the exoplanets with some false claims in the nineteenth and twentieth centuries. Finally, the first definite detection was made by Michel Mayor and Didier Queloz of the University of Geneva in 1995. In their monitoring of 142 G and K dwarf stars for over 18 months, they were able to discover a hot Jupiter orbiting 51 Pegasi using radial velocity detection method (Major and Queloz, 1995). This particular event became a turning point in the history of exoplanets and it further accelerated the search. In the following years, more planets were discovered using the radial velocity method, and alternate detection methods were also being researched and developed upon. This has also brought about tremendous instrumental advances in the field of exoplanetary detection. As a result, close to 1900 exoplanets have been discovered just in the past 20 years, and the number continues to grow on a daily basis.

Detection Methods

The majority of the detection methods that are used today are indirect methods. These techniques include astrometry, timing, microlensing, transit photometry, and radial velocity detection method (*The Exoplanet Handbook*, Introduction). Although limited, direct imaging techniques of exoplanets also exist. All of the currently known detection methods are further summarized in Figure 1, and more detail regarding the most popular detection techniques will be provided in the following sections. There are many limitations that are associated with indirect detection methods. Figure 1 below provides one such example by showing the limiting masses of the host stars for each of the detection method. Along with mass, factors such as the exoplanet’s orbital period, distance from its host star, albedo with relation to the host star, and other orbital parameters are all limiting factors for indirect detection method.

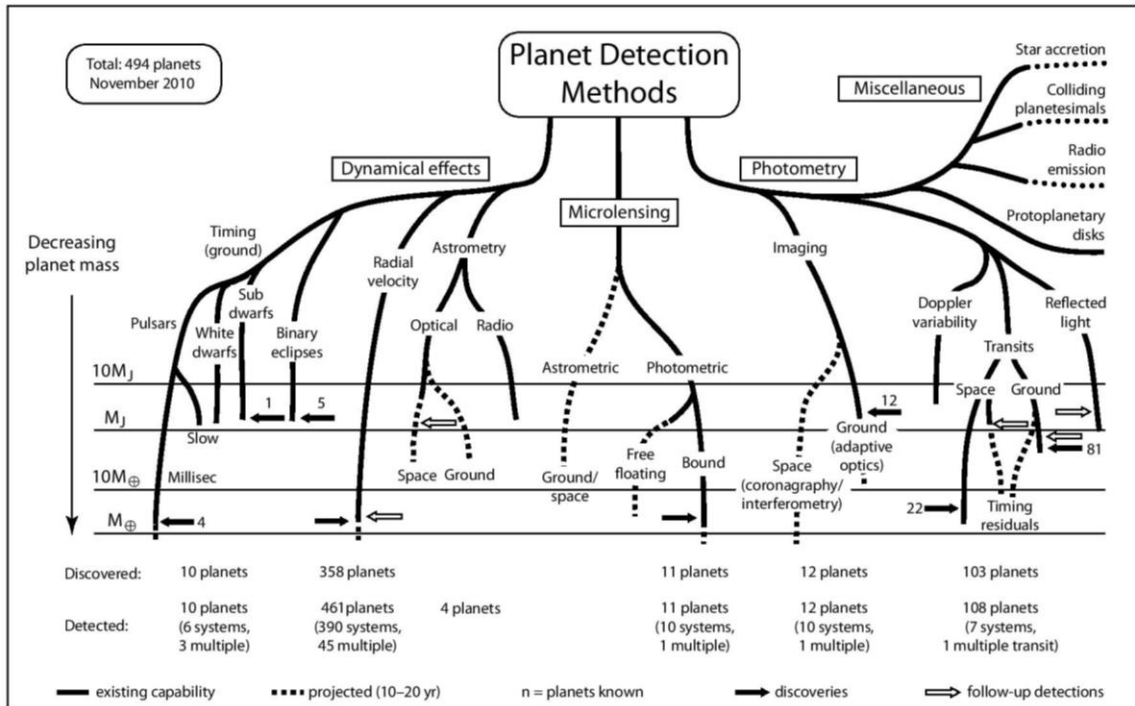


Figure 1. Flow down chart of the detection method of exoplanets (*The Exoplanet Handbook*, Introduction)

One indirect method of exoplanet discovery is astrometry. This technique relies on taking precise measurements of how the position in the sky of the star varies as the star wobbles due to the planet orbiting around the star (Townsend, 2009). This method is closely related to the radial velocity measurement method because both of the methods rely on observing the star’s motion as caused by the gravitational perturbation of a planet rotating around it. This is one of the oldest detection techniques with recordings as early as 1943 (*The Planetary Society*, 2014). Although many of the claims were declared false or left unverified, the method remained popular at that time and is also still used today. However, the fact that many of these claims were doubted despite decades of measurements shows the limitations of this technique. The process requires highly precise measurements of the motion of the star in the sky, which is very hard to achieve. Also, astrometry can only measure the angular diameter of the star’s wobble. Hence, this method is only effective when applied to low-mass stars that are close to our solar system. Another disadvantage is that the stars have to be tracked for a very long periods to detect the effects caused by the exoplanets. However, if this method is successful in finding a planet, it will also provide an accurate estimation of the planet’s mass. Very few planets have been discovered by this technique alone, and it is usually used in conjunction with radial velocity detection method.

Timing, or pulsar timing, is another indirect method of exoplanet detection. Pulsars are rapidly spinning neutron stars that are “formed during the core collapse of massive stars in a supernova explosion.” (*The Exoplanet Handbook*, Timing) These bodies are so highly magnetized, and they emit two oppositely-directed radio wave beams. As the star rotates, this

beam is swept across the sky. “If the beam intercepts the Earth once per rotation, then brief but regular pulses of radiation are seen, much like a lighthouse.” (Townsend, 2009). In presence of a planet, the star will demonstrate a wobble, and as observers, we will see a periodic change in the beam that is being displayed. By studying this change in pulsar time, information such as the lower limit on the mass of the planet and its semi-major axis can be estimated. This method is capable of detecting planets that are very small due to its sensitivity. However, any planet orbiting a pulsar would demonstrate no signs of life since they are exposed to high amounts of radiation as a result of the pulsars being formed during supernovas. Furthermore, pulsars are very rare, hence this detection method doesn’t have a large number of targets.

Micro lensing method of detection relies on Einstein’s General Theory of Relativity. This theory states that when the light of a distant star passes through another star on its path to the earth, the star in between bends the incoming light due to its gravitational field. This bending causes more light to reach earth, hence causing the star nearby the observer to act like a lens. In the presence of a planet rotating the nearby star, additional gravitational effects introduced by the exoplanet shows up as “defect in the lens.” (Townsend, 2009) This effect is easily detected when studying the brightness of the incoming light, and can help determine the mass of the planet. However, this method requires the two stars to be almost exactly aligned, which is a very a rare phenomenon. Furthermore, microlensing events are unique and do not repeat themselves, hence we only get one opportunity to gather the necessary information that can lead to exoplanet discovery. If there is such an event occurring, this method can be used to find the furthest and the smallest planets of any currently available method. (*The Planetary Society*, 2014) And, this method can be used to study thousands of target stars simultaneously, therefore it is fairly easy to detect and can lead to important information. So far, thirty-three exoplanets have been discovered using this method.

Another method of indirect detection is using transit photometry. When a planet passes between a host star and the Earth, the brightness of the star as seen from Earth is slightly dimmed. The degree of dimming as well as the time period between each successive transit can help determine the size and orbital period of the planet, although not its mass. After the launch of the Kepler mission in 2009, this method has proved to be the most effective in discovery of exoplanets. So far, it has discovered close to 1165 planets (out of the currently known 1853 planets) and enlisted thousands of other candidates. Furthermore, it can provide other information about the planet including its atmospheric composition. When the light of the star passes the planet, the planet’s atmosphere will absorb the light at different degrees. Based on this information, the absorption spectrum of the planet can be created from which the presence of different gases in the atmosphere can be deduced (*The Planetary Society*, 2014). This technique can be used to study hundreds of thousands of target stars simultaneously, and there are multiple ground and space based systems that are conducting a search using this method. Hence, it is by far the most effective method of exoplanetary discovery. However, this method does introduce many constraints, the major one being the alignment of the host star and exoplanet with Earth.

To observe the eclipse caused by the planet, we, as observers on Earth, need to have an edge-on view of the transit. This method also requires long term observation of the system to determine the orbital period of the exoplanet being observed. Moreover, this method is known for producing many false positives, particularly when a binary star is mistaken to be a planet.

The only direct way to detect exoplanets is through direct imaging. However, this method is very difficult, and sometimes even impossible. Since the planets are much smaller and dimmer than their host planets, they often tend to get lost in the glare of the stars they are orbiting. Hence, it is very hard to distinguish the planet when their image is taken. The first confirmed instance of a directly imaged exoplanet was in July 2004 when a group of astronomers imaged a planet several times the mass of Jupiter around a brown dwarf. Even then, many claim that the only reason this was possible is because the brown dwarf is fairly dim in comparison to other stars (*The Planetary Society*, 2014). Other techniques of direct imaging have also include observing infrared spectrum of the exoplanetary system, which allows the distinction of planet and the star based on the radiated heat. Although difficult, 51 planets have been directly imaged so far. The advantage of directly imaging an exoplanet is it allows us to better understand the properties of the exoplanet and its interaction within its own solar system. For this reason, there are many instruments being developed which will eventually allow the direct imaging of exoplanet. Coronagraph is one instrument that is being researched and developed upon, and can prove to be a turning point in the discovery of exoplanetary systems.

Radial Velocity Detection Method

Since the exoplanets of interest for this research are the ones that are discovered using the radial velocity, the method will be described in greater detail. Up until the launch of Kepler mission in 2009, radial velocity was the most effective method in exoplanet discovery. Like astrometry, this technique relies on the fact that the host star wobbles as a result of an orbiting planet. Due to their gravitational pull on each other, the host star and the planet both move around their center of mass (barycenter), which may or may be located inside the star. As a result, the wobble as demonstrated by the star affects the light spectrum that is emitted by the star. When the star is moving towards the observer, a blue-shift occurs whereas when the star is moving away from the observer, a red-shift occurs. By making precise measurements of the “frequency of absorption lines” (Townsend, 2009) and observing the periodicity of blue-shift and red-shift, a planet can be discovered. This method is particularly very useful when the orbital plane of the planet is edge-on as it will provide the most information from the spectrograph because the host star will be moving directly towards or away from Earth. If the orbital plane is face-on, the motion of the star will be missed completely. Usually, the planets and the orbital plane are tilted by some angle with respect of the observer. Since this tilt is not known and only a part of the spectroscopy is visible, certain information about the planet, such as its mass cannot be deduced. Another disadvantage of this method is the limitation on the type of exoplanets it can observe. During its early years, radial velocity method mostly discovered hot Jupiters. Hot Jupiters are giant exoplanets that are similar to Jupiter, but orbit their host stars in great

proximity, notably between 0.015 to 0.5 AU (Cain, 2014). As a result, these planets have short orbital period (only a couple of days) and high surface temperatures. It is easy to detect hot Jupiters using the radial velocity method because the mass as well the distance of these exoplanets has an effect on the motion of their host stars, and the larger the mass and smaller the distance, the more the effect on the star.

Many of the earlier radial velocity studies revolved around G and K main sequence (dwarf) stars (*The Exoplanet Handbook*, Radial Velocity). Their masses range from 0.7 to 1.3 times the mass of the sun, and many of them are relatively bright with stable atmospheres. Over time, the search has expanded to most late-type sequence stars, which are stars that have cooled down over time. Other type of stars being observed include M dwarfs, early-type dwarfs (new stars that are very hot), giants and subgiants, metal poor stars, and young stars. There are many programs and observatories around the world that are conducting these searches and most of the instruments conducting these searches are echelle spectrographs. These instruments include: CORALIE, which is surveying close to 1600 stars in the southern hemisphere; ELODIE, surveying more than 1000 metal-rich stars in the northern hemisphere; California and Carnegie program using Keck, Lick, and AAT telescopes to survey about 1000 stars both in the north and the south; N2K consortium using Keck, Magellan, and Subaru telescopes to survey close to 2000 high metallicity target stars. However, not all of the searches are unique in their target stars and therefore feature many replicated studies. As of 2008, the various groups had measured close to 2500 stars with masses in the range of 0.3 to 2.5 times the mass of the sun (Marcy et al, 2008). Many more have been added to the survey program in the recent years. Table 1 shows a list of target stars in conjunction with the observatories that are studying them.

Selection	Telescope/instrument	N(stars)	Start	Reference
Main sequence:				
F8–M5	ESO–CES (ended 1998)	37	1992	Endl et al. (2002)
GK, $V < 7.65$, $v \sin i < 5 \text{ km s}^{-1}$	OHP–ELODIE	324	1994	Queloz et al. (2001)
FGKM (California–Carnegie)	Keck+Lick+AAT	1040	1995	Valenti & Fischer (2005)
FGK	Lick–Hamilton	107	1995	Marcy & Butler (1998a)
F7–M5, $< 50 \text{ pc}$	Keck–HIRES	530	1996	Vogt et al. (2000)
FGKM	Lick+Keck	844	1998	Nidever et al. (2002)
FGK IV–V, $V < 8$, $\delta < -20^\circ$	AAT–UCLES	300	1998	Jones et al. (2002)
Hipparcos parallax-limited	La Silla–CORALIE	1650	1998	Tamuz et al. (2008)
F–M, metal-rich	AAT–UCLES	20	1999	Tinney et al. (2003)
F–M (N2K), metal-rich	Keck+Magellan+Subaru	2000	2004	Fischer et al. (2005, 2007)
metal-rich, Hipparcos-based	OHP–ELODIE/SOPHIE	1061	2004	da Silva et al. (2006)
low activity (Rocky Planet)	AAT–AAPS	55	2007	O’Toole et al. (2009b,a)
metal-rich (Calan–Hertfordshire)	ESO–HARPS	350	2008	Jenkins et al. (2009a)
GKM (Eta–Earth)	Keck–HIRES	230	2008	Howard et al. (2009, 2011a,b)
F8 and later	SDSS III MARVELS	10 000	2008	Ge et al. (2009)
M dwarfs:				
M2–M5, $V < 11.5$	Mt Wilson 2.5-m	65	1984	Marcy et al. (1986)
Lick/Keck	Lick+Keck	24	1994	Marcy et al. (1998)
$V < 7.5$	AAT–UCLES	7	1998	Jones et al. (2002)
CNS3, $d < 9 \text{ pc}$, $V < 15$	OHP–ELODIE/SOPHIE (N)	127	1995	Delfosse et al. (1999a)
" $d < 12 \text{ pc}$	La Silla–FEROS (S)	200	2000	Bonfils et al. (2004)
ESO survey	VLT–UVES	40	2000	Zechmeister et al. (2009)
"	VLT–UVES	26	2002	Guenther & Wuchterl (2003)
McDonald survey	HET–HRS+HJS	100	2002	Endl et al. (2003)
$d < 11 \text{ pc}$	HARPS	200	2003	Mayor et al. (2009a)
Palomar	Palomar–TEDI	100	2007	Edelstein et al. (2007)
K–M (M2K)	Keck	1600	2009	Apps et al. (2010)
Early-type dwarfs:				
early-type, B8–F7	ELODIE/SOPHIE+HARPS	185	2004	Desort et al. (2009)
Subgiants:				
subgiants	Lick+Keck	159	2006	Johnson et al. (2006b, 2010b)
Giants:				
G/K/clump giants	Lick+Keck	45	1999	Nidever et al. (2002)
"	Lick–CAT	179	1999	Hekker et al. (2006, 2008)
"	Okayama–HIDES/Subaru	300	2001	Sato et al. (2008a,b, 2010)
"	La Silla–FEROS	83	2001	Setiawan et al. (2003a,b)
" (in 13 open clusters)	HARPS	115	2003	Lovis & Mayor (2007)
" (Penn State/Torun)	HET–HRS	1000	2004	Niedzielski & Wolszczan (2008)
"	Tautenburg 2-m	62	2004	Döllinger et al. (2007, 2009)
"	SDSS III–MARVELS	1000	2008	Ge et al. (2009)
"	BOA–BOES	55	2010	Han et al. (2010)
Open clusters:				
Hyades giants	Okayama–HIDES	4	2001	Sato et al. (2007)
Hyades dwarfs	Keck+others	94	2002	Cochran et al. (2002)
13 clusters	CORALIE+HARPS	115	2003	Lovis & Mayor (2007)
Abundance-based:				
metal-poor	FEROS	70	2008	Setiawan et al. (2010)
metal-poor	Keck–HIRES	200	2003	Sozzetti et al. (2006, 2009)
metal-poor	HARPS	105	2003	Santos et al. (2007)
Young stars:				
young stars, Cha I cloud	VLT–UVES	12	2000	Joergens (2006)
young stars, 1–100 Myr	FEROS+HARPS	200	2003	Setiawan et al. (2008a,b)
Binary and multiple stars:				
CORAVEL single-lined (SB1)	ELODIE+CORALIE	101	2001	Eggenberger (2010)
wide binaries, $a = 100 - 1000 \text{ AU}$	TNG–SARG	100	2003	Gratton et al. (2003)
binary/multiple	Keck–HIRES/HET–HRS	450	2003	Konacki (2005a,b)
visual binaries	Okayama–HIDES	9	2004	Toyota et al. (2009)

Table 1. Radial velocity survey stars and corresponding observatories performing the surveys (Exoplanet Handbook, 2011)

Orbital Mechanics

A Keplerian orbit can be uniquely defined using six orbital parameters, all of which can be divided into two groups: dimensional and orientation (*Orbital Mechanics*, Keplerian Elements). The dimensional parameters are:

- Semi-major axis (a): size of the orbit
- Eccentricity (e): shape of the orbit
- Mean anomaly (M): defines where the object is with respect to the periapsis

The orientation parameters are:

- Inclination (I): tilt of the orbit relative to a reference plane; $0^\circ \leq i \leq 180^\circ$
- Longitude of ascending node (Ω): defines the location of ascending and descending orbit locations with respect to the reference plane
- Argument of periapsis (ω): defines the angle measured from the ascending node to the periapsis

Figure 2 will provide a pictorial representation of all the orbital elements described above.

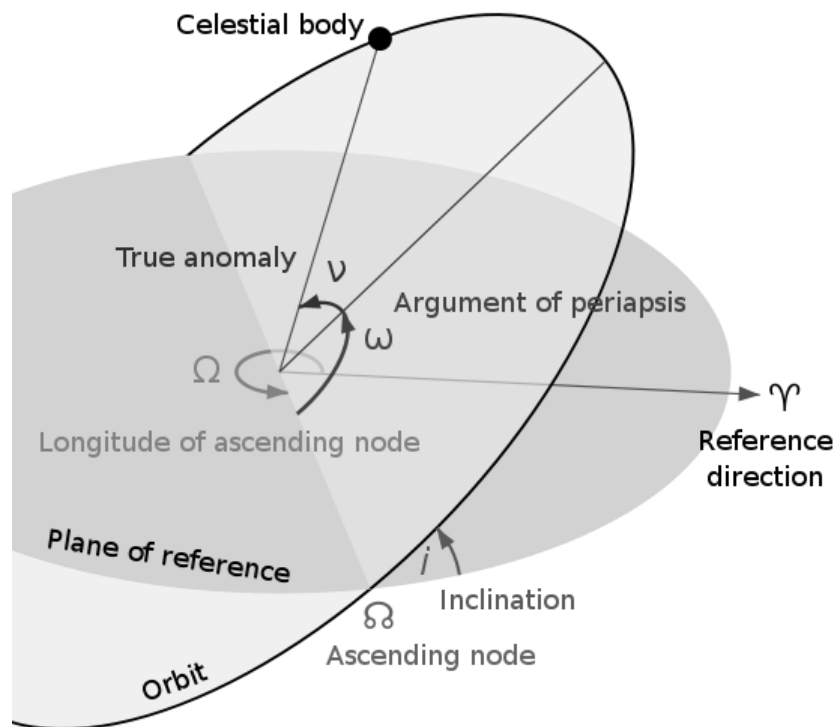


Figure 2. Representation of orbital elements (“Asteroids and Minor Planets”)

Of the six elements described above, longitude of ascending node (Ω) cannot be determined using the radial velocity measurement. Furthermore, only the combination of $a \cdot \sin(I)$ can be determined, and neither a nor I individually (*The Exoplanet Handbook*, Radial Velocity). The same restriction also applies to the measured mass of the exoplanet. The sine factor is

obtained based on the fact the observed exoplanet's orbit is probably tilted with respect to Earth. Hence, if the angle of inclination for the face-on inclination is taken to be i , the component which is in line with the observer (Earth) is $\sin(i)$ (*The Planetary Society*, 2014). Because of these type of restriction on the type of data can be gathered, the radial velocity method is usually used in conjunction with astrometry method to gather more information about the observed planet.

Coronagraph Specification

A coronagraph to directly image exoplanets has been proposed for the Wide-Field Infrared Survey Telescope-Astrophysics Focused Telescope Assets (WFIRST-AFTA), which is a 2.4-meter space telescope under development by the NASA Goddard Center. This coronagraph design is based on a hybrid design of a Lyot coronagraph (Blackwood et al, 2013). The operation of a Lyot coronagraph first begins when light enters the telescope aperture and is blocked by a secondary mirror at the center. After imaging this light, an occulting spot is placed which absorbs most of the light from the center. This is followed by another lens which again reimages the pupil causing a formation of concentrated rings of light. This image then goes through Lyot stop, and it blocks the remaining light from the central star “whilst allowing most of the light from the surrounding sources to pass through the final image, created by a final lens.” (Oppenheimer, 2003) In a hybrid design, additional components are added so that in addition to blocking the light at the center, the wavefront itself is modified. This then allows the remaining light to be placed where it can be better blocked from the Lyot stop (Trauger et al, 2012). As a result, the light from the host star is dimmed 99% while that of the exoplanet and surrounding area is only dimmed by 50%. A pictorial summary of a Lyot coronagraph process is provided in figure 3a, and the hybrid design is shown in figure 3b. If implemented, this instrument will revolutionize the direct imaging of exoplanets. This feature “would be able to detect new planets around many of the nearest stars.” (“WFIRST-AFTA Final Report”) The target exoplanets for the direct imaging purposes would be the exoplanets that are already discovered using the radial velocity method. By taking images and spectra of these exoplanets, we will be able to further understand and characterize the properties of these exoplanets. The key features of the coronagraph are given in Table 2, and it provides an insight on the limitations of planet that can be observed. The contrast and inner working angle restrictions are the ones we are most concerned with for the purposes of this research.

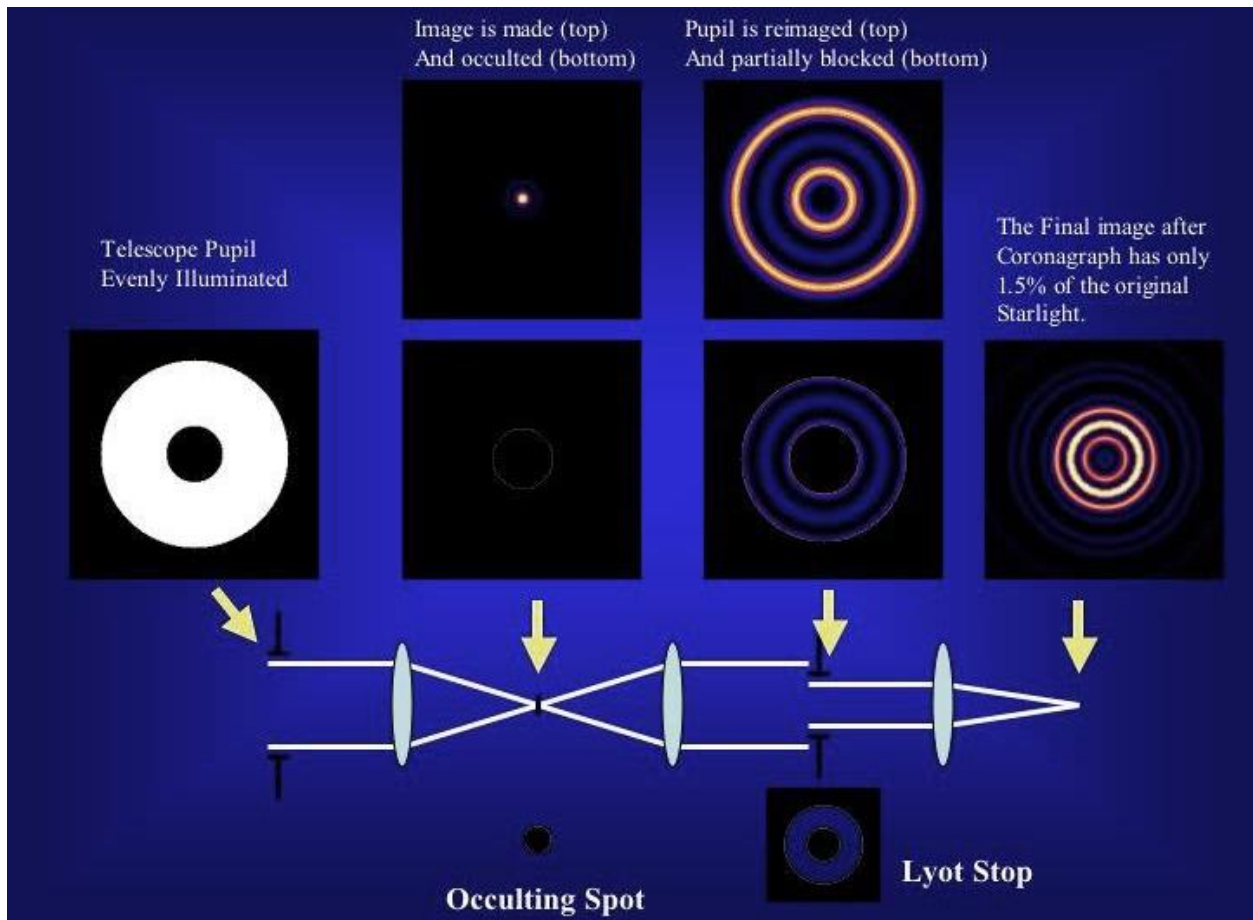


Figure 3a. Process description of a Lyot coronagraph (Oppenheimer, 2003)

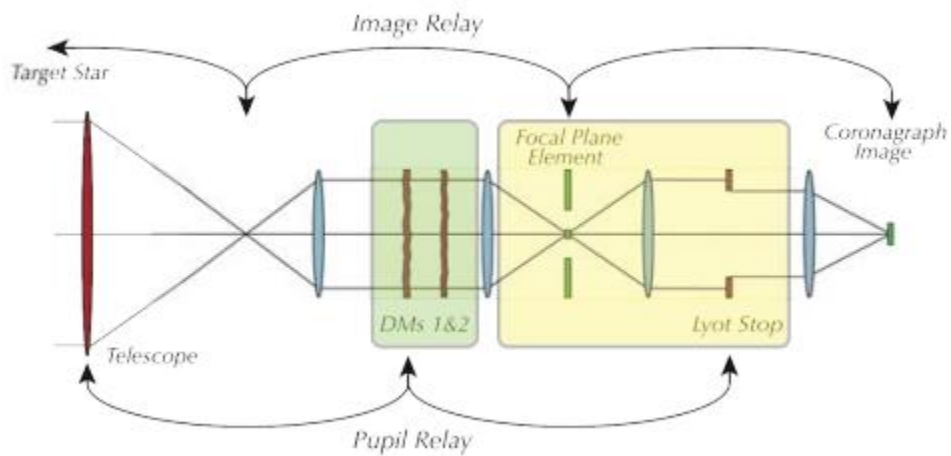


Figure 3b. Hybrid Lyot coronagraph with pupil mask where wavefront elements are given in green and coronagraph elements are given in yellow (Traugar et al., 2012)

Bandpass	400-1000 nm	Measured sequentially in five 18% bands
Inner Working Angle	100 mas	at 400 nm, $3\lambda/D$ driven by challenging pupil
	250 mas	at 1 μm
Outer Working Angle	1 arcsec	at 400 nm, limited by 64x64 DM
	2.5 arcsec	at 1 μm
Detection Limit	Contrast= 10^{-9}	Cold Jupiters. Deeper contrast looks unlikely due to pupil shape and extreme stability requirements.
Spectral Resolution	70	With IFS
IFS Spatial Sampling	17 mas	This is Nyquist for $\lambda = 400 \text{ nm}$

Table 2. Coronagraph specifications and features (“WFIRTST-AFTA Final Report”)

Methodology

The process is initiated by extracting data for all 518 radial velocity (RV) exoplanets from an online exoplanet encyclopedia, www.exoplanet.eu. From the extracted data, all of the exoplanets that don’t have information on the semi-major axis (a) and/or the eccentricity (e) are discarded as that will result in an undefined orbit for the planet. For further definition of the orbit, all of the other orbital parameters, namely the inclination (I), argument of pericenter (ω), and longitude of ascending node (Ω), are also taken into consideration. In the case where the latter three orbital parameters are not defined, we assume a distribution based on isotropically distributed orbital orientations by randomly generating values based on a presumptive prior distribution. First, we consider the value of I which can range from 0° to 180° or from 0 to π radians. As the nature of the inclination is sinusoidal, an inverse cosine function on a uniformly distributed random number between -1 and 1 is used to approximate the inclination of the orbit. For ω and Ω , both of these values can vary anywhere from 0 to 2π uniformly. Therefore, for these values, a random number is generated between 0 and 1, and then multiplied by 2π to get an approximation.

The given orbital parameters include an error estimate associated with them. To make a proper judgment on all of the exoplanet’s possible orbits, these orbital parameters are taken to be normally distributed with the mean as the value given and the error estimate as the standard deviation. This method was applied to the given values of a , e , I and ω .

The ultimate purpose of simulating the possible orbits is to determine the visibility times and their distribution. Therefore, it is necessary to simulate an appropriate number of orbits and appropriate number of time intervals within the orbits to get a proper distribution. Although it is

beneficial to have higher number of sample points, other considerations such as computer memory allocation and simulation time has to be taken into consideration. Therefore, we choose to simulate 450 orbits with 250 intervals within each orbit. Although the overall shape of the distribution converges at a much smaller sample size, the chosen values provide a good balance between providing appropriate number of samples and a reasonable simulation time.

Following the extraction and/or estimation of the orbital parameters, further calculations are made to fully determine the position and velocity parameters of all the possible orbits. First, values such as gravitational parameter (μ), semi-minor axis (b), mean motion (n) are calculated using the orbital parameters and the given mass of the exoplanet. The following equations, as derived from the Orbital Mechanics book, were used to determine those values:

$$\mu = G(M_p + M_s)$$

$$b = a\sqrt{1 - e^2}$$

$$n = \sqrt{\frac{\mu}{a^3}}$$

where G is the gravitational constant, M_p and M_s are mass of the planet and the host star respectively. Then, to find all the time and position of the exoplanet during its one orbit, the Newton-Raphson method is utilized to determine eccentric anomaly E for values of the mean anomaly M between from 0 to 2π to define a full orbit. As stated above, we are simulating 250 of M between 0 and 2π . Newton-Raphson is method of linear approximation that effectively finds the roots of a real function. For any variable x and its function $f(x)$, the Newton-Raphson method is carried out as follows:

$$x_{n+1} = x_n - \frac{f(x_n)}{f'(x_n)}$$

To start the Newton-Raphson process, we need an initial guess on the value of the variable x_0 so that we can estimate the value of x_1 . For each successive x_{n+1} thereafter, we use our previously derived value as x_n . The value of the variable x gets more accurate with each step, and converges to the actual value over time. We stop when the difference between x_{n+1} with x_n is negligible, which implies that value of x has converged to the actual value.

To implement the Newton-Raphson method on the eccentric anomaly E , the initial value of E is taken to be:

$$E_0 = \begin{cases} \frac{M}{1 - e} & \text{if } \left(\frac{M}{1 - e}\right) < \sqrt{\frac{6(1 - e)}{e}} \\ \left(\frac{6M}{e}\right)^{1/3} & \text{else} \end{cases}$$

Using this initial condition and the function for mean anomaly $M = E - e \sin(E)$, the Newton-Raphson method can be used to derive the values for E for the full orbit.

Once we have the values of the eccentric anomaly E , we can directly define the inertial orbital position and velocity using equivalent Euler angles approximation method. This calculation can be carried out as follows:

$$\mathbf{r} = \mathbf{A}(\cos E - e) + \mathbf{B}\sin(E)$$

$$\mathbf{v} = \dot{E}[-\mathbf{A}\sin(E) + \mathbf{B}\cos(E)]$$

where

$$\mathbf{A} = a \begin{bmatrix} -\sin(\Omega) \sin(\omega) \cos(I) + \cos(\Omega) \cos(\omega) \\ \sin(\Omega) \cos(\omega) + \sin(\omega) \cos(I) \cos(\Omega) \\ \sin(I) \sin(\omega) \end{bmatrix}$$

$$\mathbf{B} = b \begin{bmatrix} -\sin(\Omega) \cos(I) \cos(\omega) - \sin(\omega) \cos(\Omega) \\ -\sin(\Omega) \sin(\omega) + \cos(I) \cos(\Omega) \cos(\omega) \\ \sin(I) \cos(\omega) \end{bmatrix}$$

We can then easily solve for the orbital position and velocity of the exoplanet.

Once the information on the radius of the exoplanets is extracted, the data can be filtered further based on the given specifications for WFIRST-2.4 coronagraph. The radius of the visibility can be determined based on the inner working angle (IWA) of the coronagraph and the distance from our solar system to the host star. And, this IWA radius can be compared with the projection of the orbital radius into the $-s_3$ plane, which is the region we can observe and is further shown in figure 4. Using this method, two separate listings of visible planets are gathered – for the IWA of 200 milliarcseconds and 100 milliarcseconds. The visibility percentage of each planet is determined by taking the ratio of the length of the array of visible radii versus length of the array of all of the possible radii. The filtering process is conducted based on a minimum visibility threshold of 5%. Given the sample size as given above, this visibility threshold ensures that proper visibility distribution is generated for each planet.

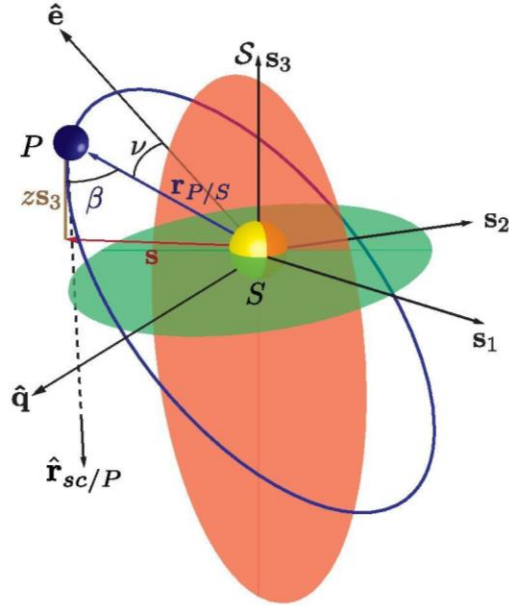


Figure 4. Planetary orbit schematic where observer sc lies along $-s_3$ axis (Savransky, 2013)

For all the planets that are visible with either of the two inner working angles, we can extract their visibility times. We can also generate a radial velocity profile using the third (z) component of the velocity. The visibility times can then be compared to the times of minimum and maximum radial velocity points, by subtracting the corresponding minimum or maximum radial velocity times from the visible times. The times can then be normalized to range from 0 to 1 representing one full orbital period, and we can generate histograms to view the distribution of visibility. This step can be completed for both individual planets as well as for all the planets together so that conclusions can be drawn about the overall visibility times.

Following the determination of the best times for detection, we can look at specific time ranges and determine the number and specific time of opportunities to image each exoplanet. This can be carried out by projecting the radial velocity of the exoplanets, which is easily undertaken as these are periodic functions. The time at periastron for each of the exoplanets are given, and the orbital period can be calculated while determining the position and velocity. Hence, using these two pieces of information, the radial velocity of the exoplanet can be projected both to the future and the past. Given a specific time range, it can be converted to a Julian time and plotted alongside the radial velocity profiles and their corresponding time to determine the best suitable times for visibility.

Among other things, there are also contrast limitations that the exoplanets have to surpass. We considered some test contrast limitations, and determined which of the exoplanets would be visible given the criteria. The contrast for the exoplanet themselves is expressed using what Brown calls the “delta magnitude” (Brown, 2005). This delta magnitude is expressed as follows:

$$\Delta mag = -2.5 \log \left[p \Phi(\beta) \left(\frac{R}{r} \right)^2 \right]$$

where p is the albedo of the planet, and it is taken to be 0.5 assuming the exoplanets are Jupiter-like. The radius of the exoplanet itself is R , and r expresses the projected radius on the s_3 plane from the host star to the exoplanet. Phase angle is given by β which is the same β as shown in figure 4 above; finally $\Phi(\beta)$ is the Lambert phase function and is defined as follows:

$$\Phi(\beta) = \frac{\sin \beta + (\pi - \beta) \cos \beta}{\pi}$$

This delta magnitude of the exoplanet was compared with the given contrast limitation by taking the $-2.5 \log_{10}$ of the given contrast values. Then, each of these can be plotted versus the given radius specifications and exoplanetary systems radius respectively to obtain final comparison plots.

Results and Discussion

After the filtration process of only extracting the visible exoplanets, we found only 22 planets to be visible with IWA of 200 mas and 63 to be visible with the IWA of 100 mas. Among the 22 that are visible for the IWA of 200 mas, the visibility percentage is provided in Table 3 below. :

Planet	Visibility %	Planet	Visibility %
eps Eridani b	86.61	HIP 70849 b	11.19
GJ 832 b	71.87	HD 99492 c	33.42
GJ 433 c	50.31	HD 154345 b	20.74
GJ 849 b	21.97	HD 87883 b	28.92
55 Cnc d	62.94	HD 217107 c	35.88
ups And d	11.91	GJ 328 b	19.41
ups And e	48.11	HD 142 c	38.44
47 Uma c	22.59	HD 114613 b	19.03
47 Uma d	72.94	HD 134987 c	22.81
GJ 317 c	89.09	HD 190360 b	24.9
mu Ara e	42.01	HD 219077 b	22.83

Table 3. Visibility percentage for each visible exoplanet for 200 IWA

The corresponding data for these 22 exoplanets show that many of them correspond to systems that are fairly close to our solar system, with the maximum distance being 29.35 parsecs. Most of these exoplanets have host stars that are between 3 and 22 parsecs away from our solar system. The semi-major axis of these exoplanets range between 2.55 and 11.6 AU. They also

show a range of varying eccentricities, with the maximum being 0.702. A tabled detail of the exoplanets can be found in the Appendix.

We can first look at the overall visibility for all the planets taking time $t=0$ to be either the minimum or the maximum velocity case. Figure 5a and 5b show the distributions if we take $t=0$ to correspond to minimum and maximum velocity respectively.

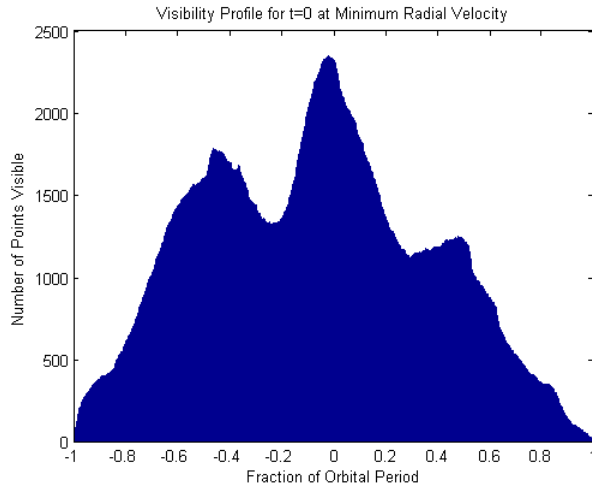


Figure 5a. Visibility distribution for $t=0$ at minimum radial velocity

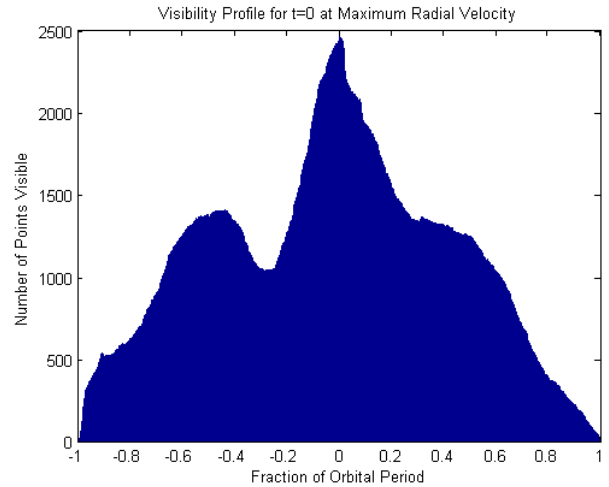


Figure 5b. Visibility distribution for $t=0$ at maximum radial velocity

Both of these distribution profiles show a very clear peak corresponding to the minimum and maximum radial velocity. This tells us that the best time to imagine the exoplanets to ensure visibility is during their minimum and maximum radial velocity. Although we see a symmetric profile appearing around the $t=0$ point, we should note that it is not perfectly symmetric. To further explore why this is the case, we can carry out test cases on the orbital parameters. We first look at the edge-on case of the exoplanets, which occurs when inclination is 90 degrees. To get more of a distribution, we consider the case where the inclination ranges from 45 to 135 degrees. The results are shown in figure 6a and 6b.

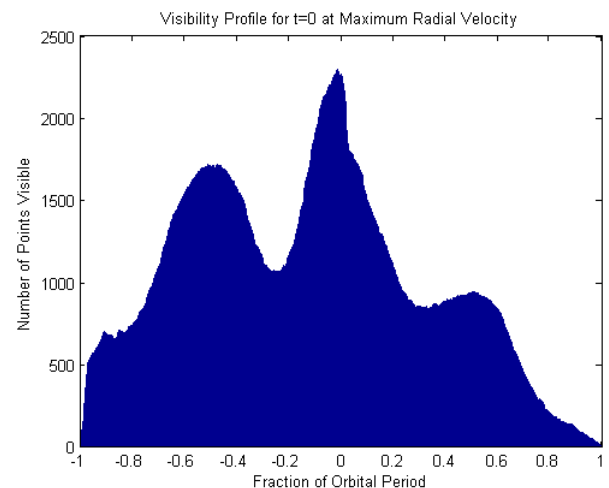
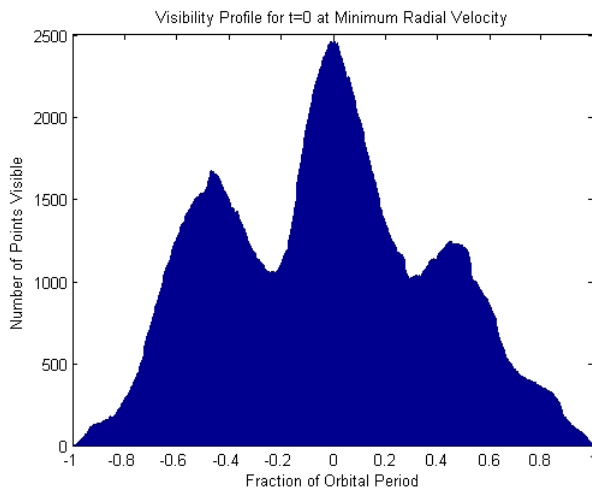


Figure 6a. Visibility profile at $t=0$ at minimum radial velocity for inclination from 45° to 135°

Figure 6b. Visibility profile at $t=0$ at maximum radial velocity for inclination from 45° to 135°

The resulting profile is still asymmetric; hence we consider further restrictions on the orbital parameters. The next case is when $e = 0$ and $\omega = 0$. The resulting profiles are shown in figure 7a and 7b.

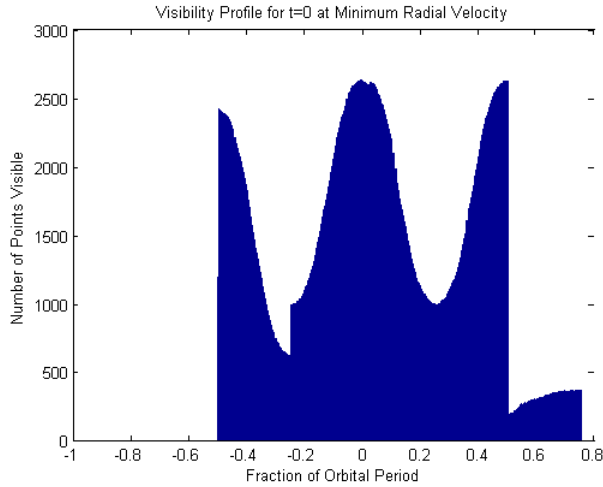


Figure 7a. Visibility profile at $t=0$ at minimum radial velocity for $e = 0$ and $\omega = 0$

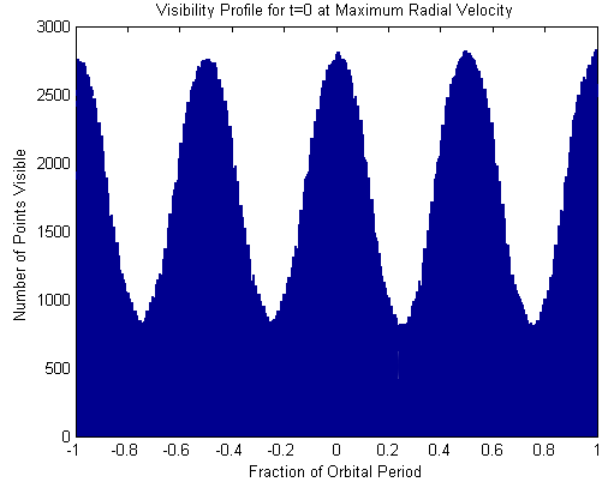


Figure 7b. Visibility profile at $t=0$ at maximum radial velocity for $e = 0$ and $\omega = 0$

Although we get symmetric profile when we consider $t=0$ at maximum radial velocity, it's not the case for the minimum radial velocity. We can further explore the reason behind this asymmetric nature by considering the visibility profile of planets individually and we discover that the reason behind is due to exoplanets which have a high error estimate in semi-major axis in comparison to the value of semi-major axis itself. The visibility distribution for $t=0$ at minimum velocity for HIP 70849b for the test case is shown in figure 9, while that for other planets is shown in figure 10.

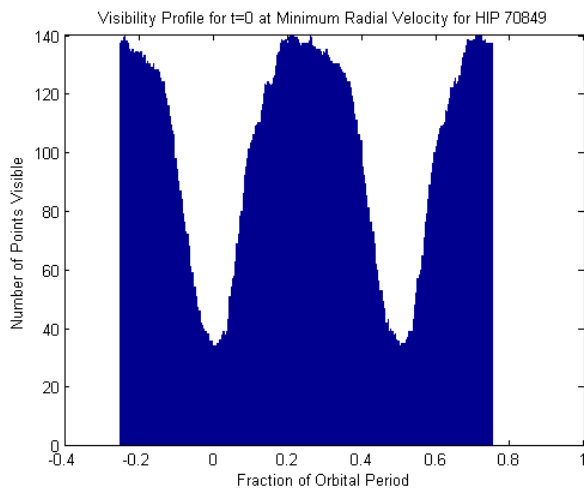


Figure 9. Visibility distribution for $t=0$ at

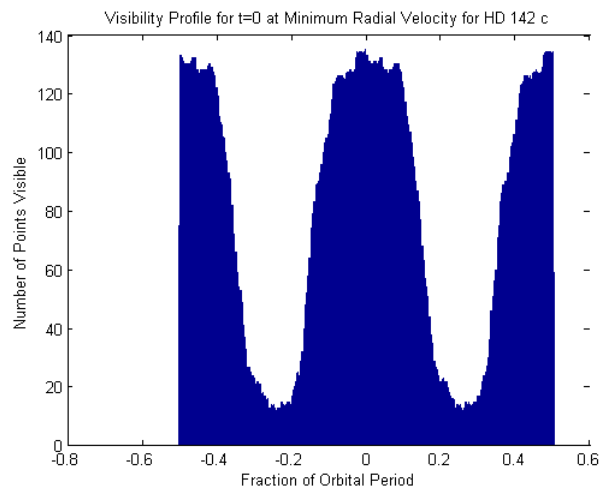


Figure 10. Visibility distribution for $t=0$ at

minimum velocity for HIP 70849b

minimum velocity for a sample planet (HD 142c)

We see that although the symmetric behavior, the profile is translated over by .2 fraction of the orbital period. Therefore, we carry out another test case by eliminating HIP 70849b, and the result is as shown in figure 11a and 11b.

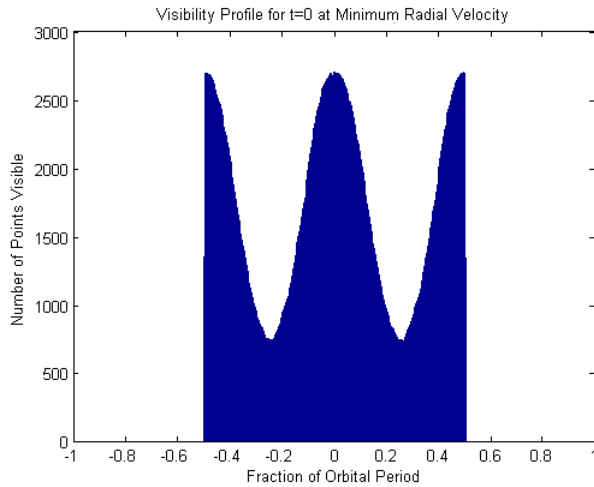


Figure 11a. Visibility distribution for $t=0$ at minimum radial velocity after eliminating HIP 70849b

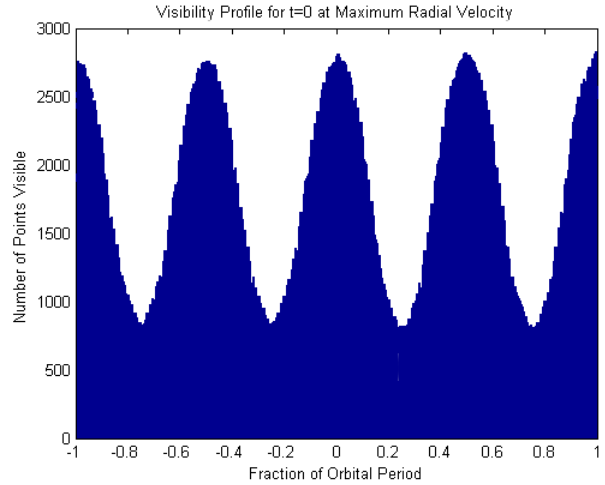


Figure 11b. Visibility distribution for $t=0$ at maximum radial velocity after eliminating HIP 70849b

We can further explore other test cases by setting only $\omega=0$. As a result, we get the profiles as shown in figure 12a and 12b.

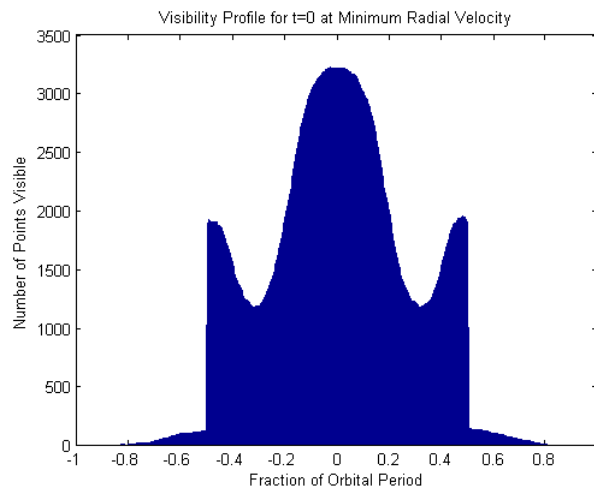


Figure 12a. Visibility distribution for $t=0$ at minimum radial velocity at $\omega=0$

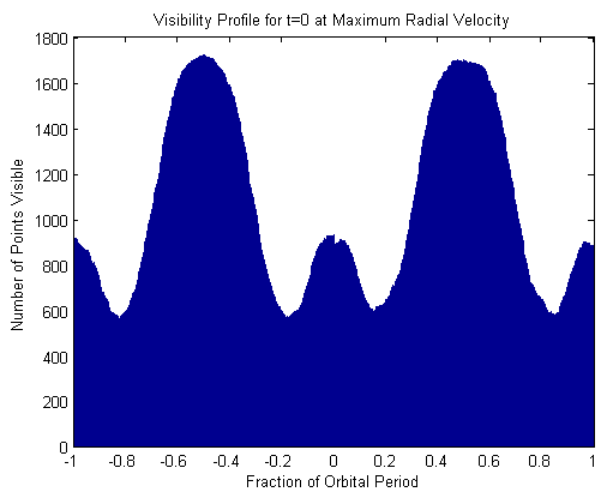


Figure 12b. Visibility distribution for $t=0$ at maximum radial velocity at $\omega=0$

Based on the test cases above, we can make some conclusion regarding the asymmetric nature of the visibility profiles. The major contributor is the argument of periastron (ω). Many of

the exoplanets that we are considering (20 out of 22) provide a value for ω , and this set definition results in the asymmetric nature as seen above. Other factors include the inclination, eccentricity, and also the error estimate of the semi-major axis in comparison to the given value. However, it is still very clear that the best times to image the exoplanets is during their maximum and minimum radial velocity.

Since we know that the minimum and maximum radial velocity is the ideal time for imaging, we can determine the number of such opportunities within the desired time range for each exoplanet. For our purposes, we chose to look at a six-year time frame from 01/01/2022 to 01/01/2028. One of the sample exoplanet is ups And d, and the radial velocity profile and the time range for this exoplanet is shown in figure 13. This image clearly shows that there are three opportunities of imaging (or three minimum and maximum radial velocity points) within the time frame (denoted by vertical blue lines in figure 13). The specific times are on July 29, 2023 at 10:20 PM and January 16, 2027 at 5:44 PM for minimum radial velocity, and on September 28, 2024 at 12:13 PM for maximum radial velocity.

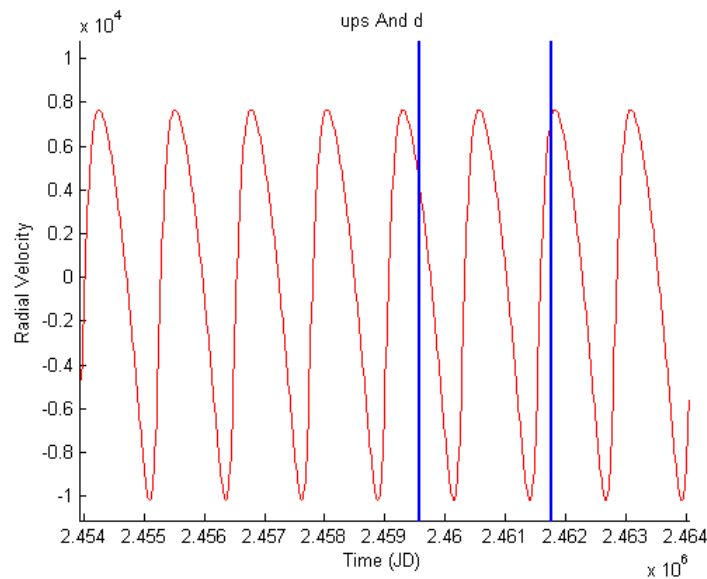


Figure 13. Time range (blue lines) from 01/01/2022 to 01/01/2028 and the radial velocity profile of ups And d within that time range

Other exoplanets are examined in a similar manner, and another example exoplanet's resulting profile is shown in figure 14. This planet is HD 219077b, and as can be seen from the figure, we barely only get one opportunity to image this exoplanet with the maximum radial velocity point occurring just within the time frame. The specific time for imaging is on November 15, 2026 at 6:43 PM for maximum velocity. Similar profiles for other exoplanets are presented in the Appendix C.

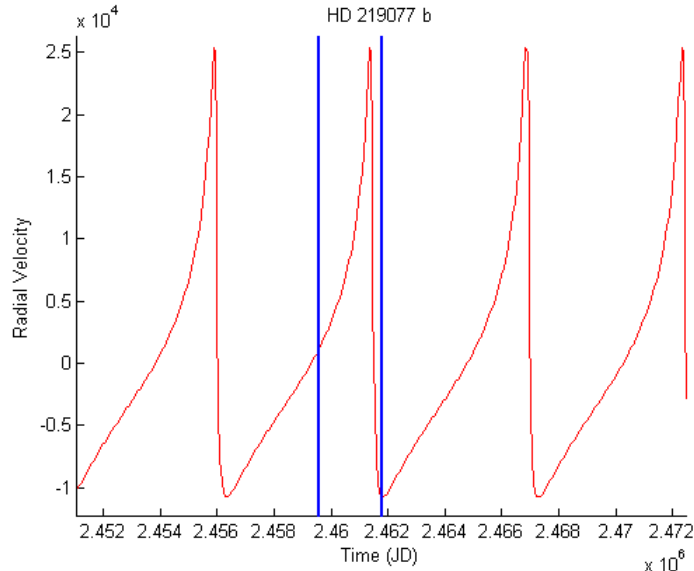


Figure 14. Time range (blue lines) from 01/01/2022 to 01/01/2028 and the radial velocity profile of HD 219077b within that time range

It is possible that there may not be an opportunity to image the exoplanet at all during a certain time range. One such example is shown in figure 15, and it looks at exoplanet 47 Uma d. The orbital period of this exoplanet is much larger than six years, hence in the six-year time period, neither the instance of minimum nor the maximum velocity occur. Hence, in this case, we wouldn't get a proper opportunity to image 47 Uma d within this time period.

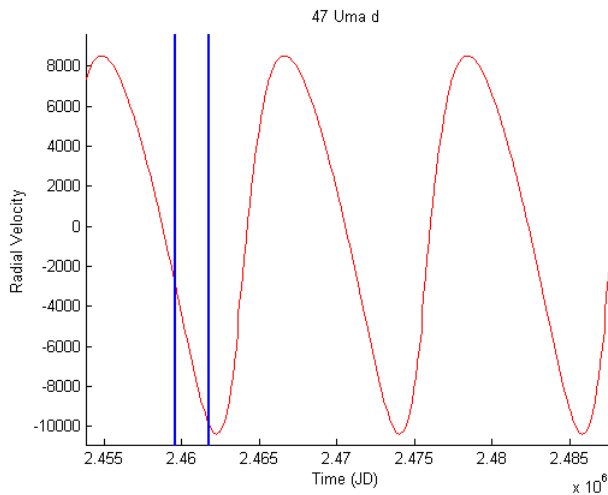


Figure 15. Time range (blue lines) from 01/01/2022 to 01/01/2028 and the radial velocity profile of 47 Uma d within that time range

Along with examining specific time ranges, the contrast limitations were also considered. The figures for ups And d and HD 219077b are shown in figure 16a and 16b. The green curve as shown is limiting delta magnitude of the contrast curve, and the red curve shows the delta magnitude of the planet itself. Any red curve above the green curve represents the planet

surpassing the contrast limitation, and both of the exoplanets we are considering are well above the contrast limitation. These curves for all the exoplanets can be found in the Appendix D.

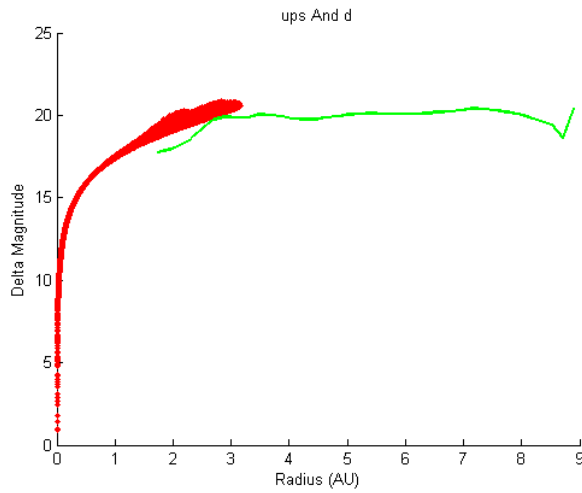


Figure 16a. Limiting and ups And d exoplanet's contrast curves

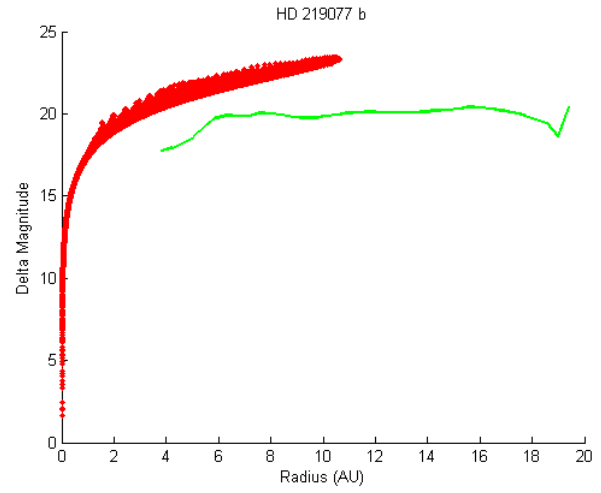


Figure 16b. Limiting and HD 219077b exoplanet's contrast curves

Conclusion

The primary objective of this research was to determine the best suitable times to image some of the exoplanets that were previously discovered using the radial velocity method. The specifications from the proposed coronagraph for WFIRST-AFTA was taken in conjunction with the orbital parameters of the exoplanets to first determine which of the exoplanets would actually be visible given the coronagraph limitations. Out of the 534 known radial velocity exoplanet, we discovered that only 22 can be directly imaged for IWA of 200 mas. Then, using the simulated orbits and determining the position and velocity of the exoplanet throughout its orbit, we were able to determine at which point of its radial velocity it is most likely to be detected. Based on the results, we can conclude that the minimum and maximum radial velocity points are the most suitable times to directly image the exoplanets. Given this knowledge and given a specific desired time range to image the exoplanets, the radial velocity can be projected forwards or backwards in time to determine the exact time and number of opportunities, if there are any minimum or maximum radial velocity points within that time frame. For exoplanets with large orbital period, longer time ranges will be needed to get at least one opportunity of minimum or maximum radial velocity while for those with shorter period, there may be multiple such instances within a time frame as short as six years. Furthermore, we were also to develop a method to consider contrast limitations on the exoplanets, and determine which of the exoplanets can be imaged for various given contrast specifications. All of the code that is generated, particularly for time range and contrast limitation considerations, can be easily altered to study other time range and contrast limitations.

References

- "Asteroids and Minor Planets." *Senior Project*. UCLA Astro, 2010. Web.
- Blackwood, Gary, and Kevin Grady. "AFTA Coronagraph Working Group Recommendation to Astrophysics Division." (n.d.): n. pag. Jet Propulsion Laboratory (JPL), California Institute of Technology, 13 Dec. 2013. Web.
- Brown, Robert A. "Single-Visit Photometric and Obscurational Completeness." *The Astrophysical Journal*. 7 Jan. 2005. Web.
- Butler, R. P., G. W. Marcy, E. Williams, C. McCarthy, P. Dosanjh, and S. S. Vogt. "Attaining Doppler Precision of 3 M S-1." June 1996. Web.
- Cain, Fraser. "What Are Hot Jupiters?" *Universe Today*, 12 Feb. 2014. Web.
- Carlotti, A., R. Vanderbei, and N. J. Kasdin. "Optimal Pupil Apodizations of Arbitrary Apertures for High-contrast Imaging." *Optics Express* 19.27 (2011): 26796. High Contrast Imaging Laboratory, Mechanical & Aerospace Engineering, Princeton University, 2011. Web.
- Chobotov, Vladimir A. *Orbital Mechanics*. Reston, VA: American Institute of Aeronautics and Astronautics, 2002. Print.
- Cumming, Andrew. "Detectability of Extrasolar Planets in Radial Velocity Surveys." Nov. 2004. Web.
- "Extrasolar Planets." *Department of Physics and Astronomy*. University of Leicester, 2012. Web.
- Harris, David. "Dark Energy and Exoplanets Top List of Astronomy Priorities | WIRED." *Wired.com*. Conde Nast Digital, 13 Aug. 2010. Web. 1 Dec. 2014.
- "Keplerian Elements." Rutgers University, 2009. Web.
- Lowman, Andrew E., John T. Trauger, Brian Gordon, Joseph J. Green, Dwight Moody, Albert F. Niessner, and Fang Shi. "High Contrast Imaging Testbed for the Terrestrial Planet

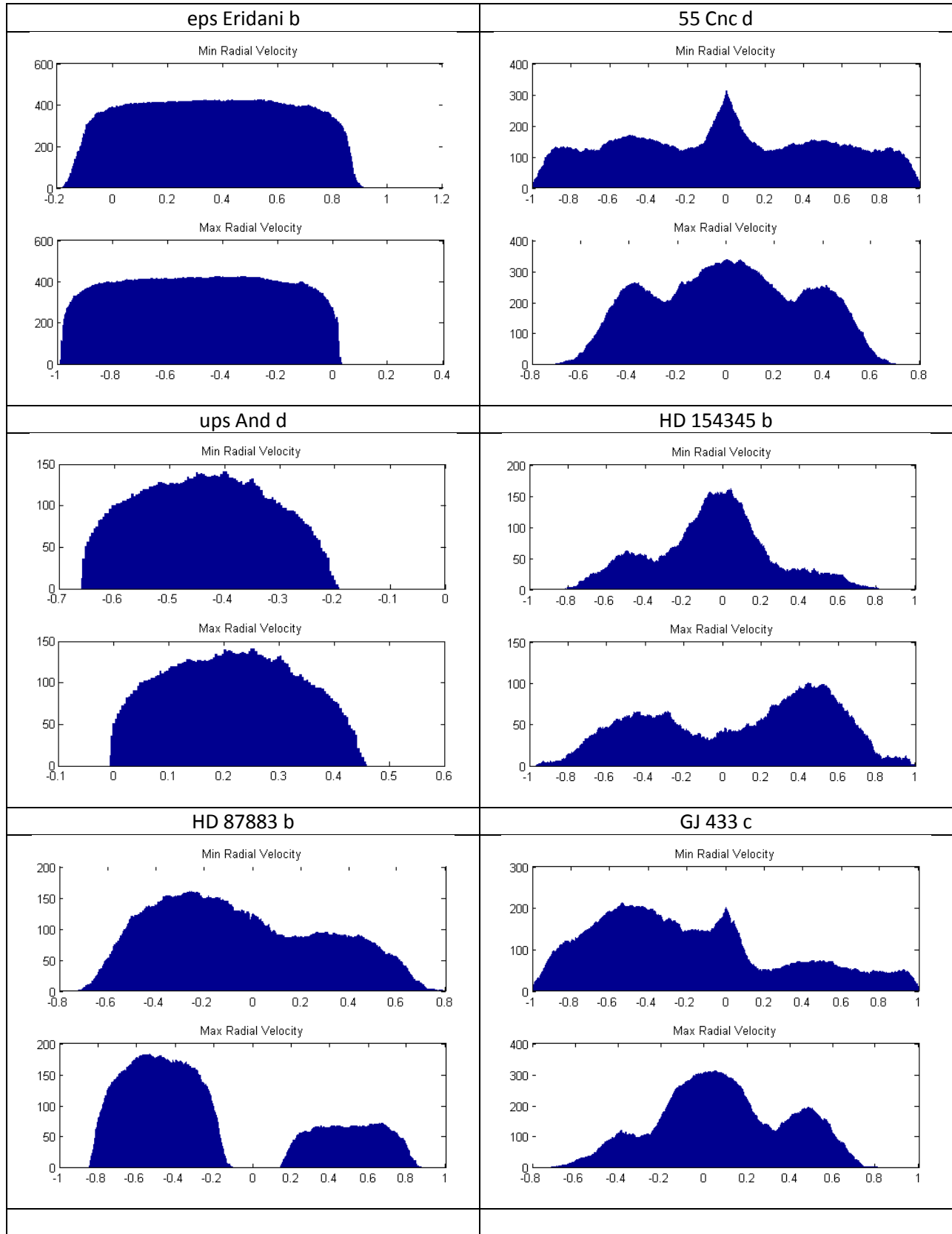
- Finder Coronagraph." (2014): n. pag. Jet Propulsion Laboratory (JPL), California Institute of Technology, 2014. Web.
- Newman, Phil, and Neil Gehrels. "WFIRST-AFTA." *Goddard Space Flight Center*. National Aeronautics and Space Administration, 21 Nov. 2014. Web.
- Oppenheimer, Ben R. "Coronagraphy." *The Lyot Project*. American Museum of Natural History, 2003. Web.
- "Orbital Elements." *Human Space Flight (HSF)*. National Aeronautics and Space Administration, 30 Oct. 2010. Web.
- Perryman, M. A. C. *The Exoplanet Handbook*. Cambridge, UK: Cambridge UP, 2011. Print.
- Savransky, Dmitry. *Space Mission Design for Exoplanet Imaging*. 2013. Web.
- "Radial Velocity." *The Planetary Society Blog*. N.p., 2014. Web.
- Townsend, Rich. "The Search for Extrasolar Planets." *Mad Star*. N.p., 13 Oct. 2009. Web.
- Trauger, John, and AFTA Coronagraph Design Team. "High Contrast Imaging Testbed (HCIT) at JPL." (n.d.): n. pag. California Institute of Technology, 2014. Web.
- Trauger, J. T., et al, "Complex apodization Lyot coronagraphy for the direct imaging of exoplanet systems: design, fabrication, and laboratory demonstrations", Proc. SPIE 8442, paper 84424Q (2012)
- WFIRST-2.4: What Every Astronomer Should Know*. 2013. Web.
- "Wide-Field InfraRed Survey Telescope-Astrophysics Focused Telescope Assets WFIRST-AFTA Final Report." 24 May 2013. Web.

Appendix

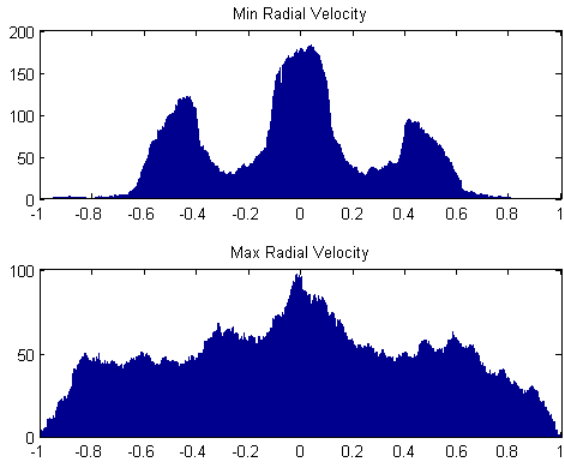
Appendix A – Characteristics of visible exoplanets

# name	mass	mass_error_min	mass_error_max	semi_m ajor_axis	semi_major_a xis_error_min	semi_major_a xis_error_max	eccentricity	eccentricity_ error_min	eccentricity_ error_max	inclination	inclination_ error_min	inclination_ error_max	omega	omega_e ror_min	omega_er ror_max	star_name	star_distance	star_mass
ups And e	1.059	0.028	0.028	5.2456	0.00067	0.00067	0.00536	0.00044	0.00044				367.3	2.3	2.3	ups And	13.47	1.27
ups And d	10.19			2.55	0.042	0.042	0.274	0.0196	0.0196	24	1	1	240.8			ups And	13.47	1.27
55 Cnc d	3.835	0.08	0.08	5.76	0.06	0.06	0.025	0.03	0.03	53	6.8	6.8	181.3	32	32	55 Cnc	12.34	0.905
HD 87883 b	12.1	10	9.2	3.6	0.08	0.08	0.53	0.12	0.12	8.5	3.7	3.7	191	15	15	HD 87883	18.1	0.82
HD 219077 b	10.39	0.09	0.09	6.22	0.09	0.09	0.77	0.003	0.003				57.61	0.42	0.42	HD 219077	29.35	1.05
47 Uma c	0.54	0.073	0.066	3.6	0.1	0.1	0.098	0.096	0.096				295	160	160	47 Uma	13.97	1.03
HD 99492 c	0.36	0.02	0.02	5.4	0.1	0.1	0.106	0.006	0.006				38	2	2	HD 99492	18	0.83
HD 114613 b	0.48	0.04	0.04	5.16	0.13	0.13	0.25	0.08	0.08				244	5	5	HD 114613	20.67	1.364
HD 190360 b	1.502	0.13	0.13	3.92	0.2	0.2	0.36	0.03	0.03				12.4	9.3	9.3	HD 190360	15.89	1.04
GJ 328 b	2.3	13	13	4.5	0.2	0.2	0.37	0.05	0.05							GJ 328	19.8	0.69
GJ 849 b	0.9	0.05	0.05	2.35	0.22	0.22	0.04	0.02	0.02				351	60	60	GJ 849	9.1	0.49
eps Eridani b	1.55	0.24	0.24	3.39	0.36	0.36	0.702	0.039	0.039	30.1	3.8	3.8	47	3	3	eps Eridani	3.2	0.83
HD 217107 c	2.49	0.25	0.25	5.27	0.36	0.36	0.517	0.033	0.033				198.6	6	6	HD 217107	19.72	1.02
GJ 832 b	0.64	0.06	0.06	3.4	0.4	0.4	0.12	0.11	0.11				304	38	38	GJ 832	4.94	0.45
HD 154345 b	1	0.3	0.3	4.3	0.4	0.4	0.26	0.15	0.15	50	26	26	-14	60	60	HD 154345	18.06	0.88
HD 142 c	5.3	0.7	0.7	6.8	0.5	0.5	0.21	0.07	0.07				250	20	20	HD 142	20.6	1.1
HD 134987 c	0.82	0.03	0.03	5.8	0.5	0.5	0.12	0.02	0.02				195	48	48	HD 134987	22.2	1.07
47 Uma d	1.64	0.48	0.29	11.6	2.9	2.9	0.16	0.16	0.16				110	160	160	47 Uma	13.97	1.03
HIP 70849 b	9	6	6	10	5.5	5.5	0.6	0.13	0.13							HIP 70849	24	0.63
GJ 317 c	2	0	0	30	10	10	0.81	0.2	0.2				210			GJ 317	15.1	0.42
GJ 433 c	0.14			3.6	0.3	0.3	0.17	0.09	0.09				-154	36	36	GJ 433	9.04	0.48
mu Ara e	1.814			5.235	0.15	0.15	0.0985	0.0627	0.0627				57.6	43.7	43.7	mu Ara	15.3	1.08

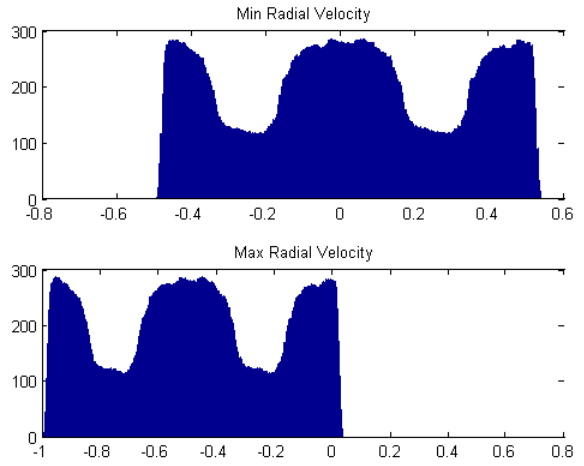
Appendix B – Visibility time profiles for each exoplanet



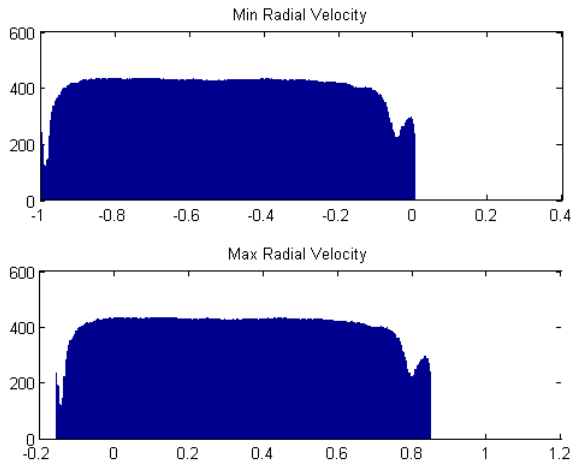
GJ 849 b



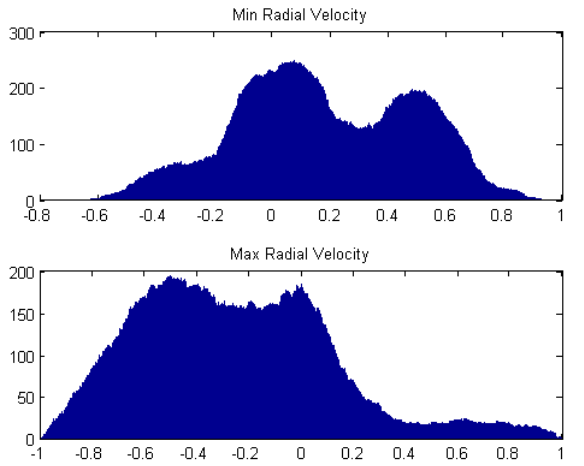
Ups And e



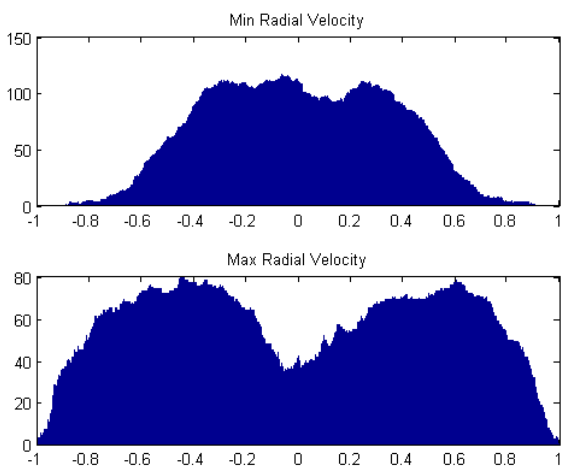
GJ 317 c



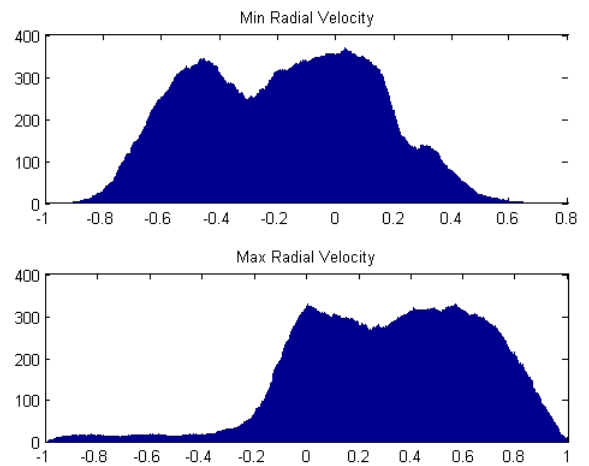
Mu ara e



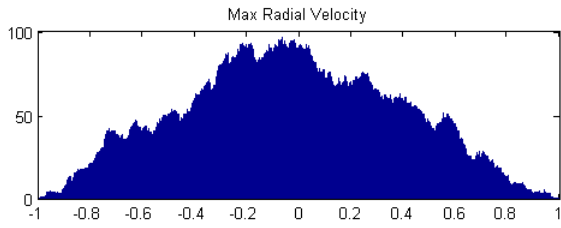
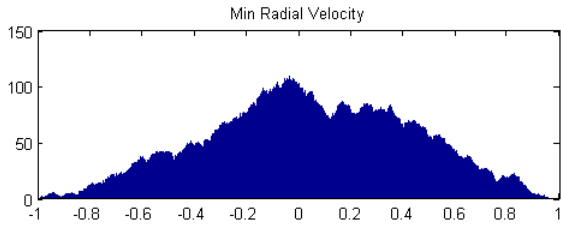
HIP 70849b



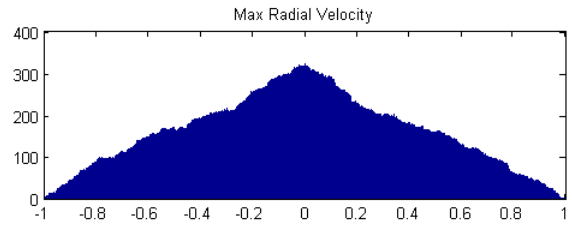
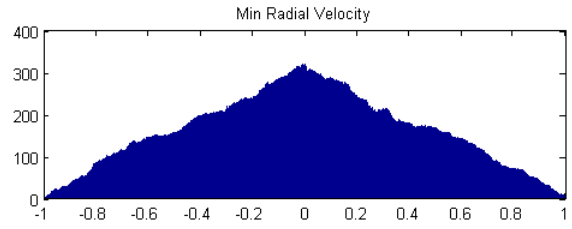
GJ 832 b



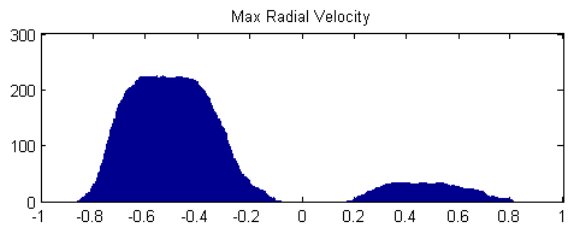
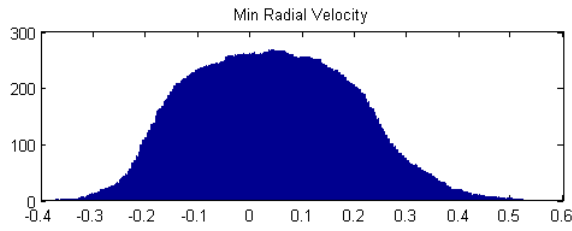
47 Uma c



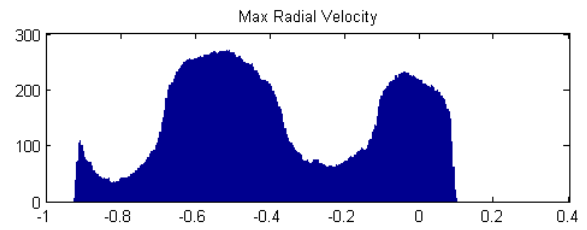
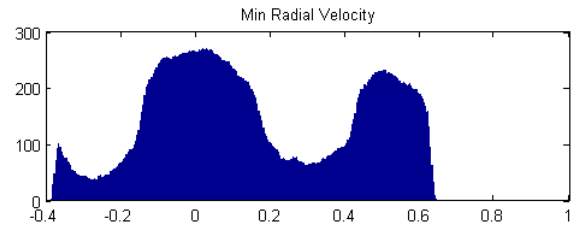
47 Uma d



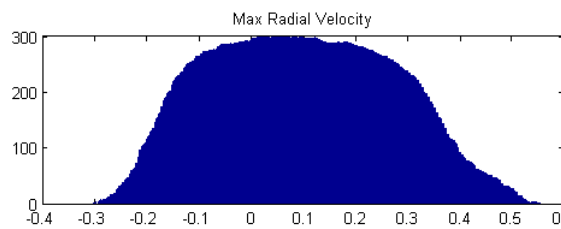
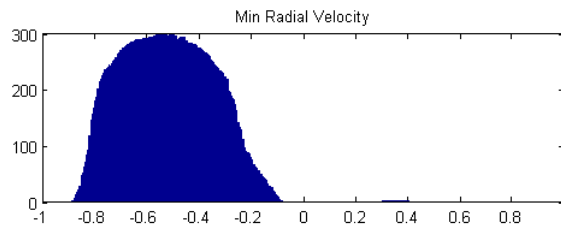
HD 190360



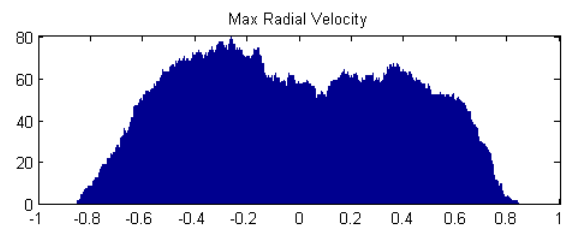
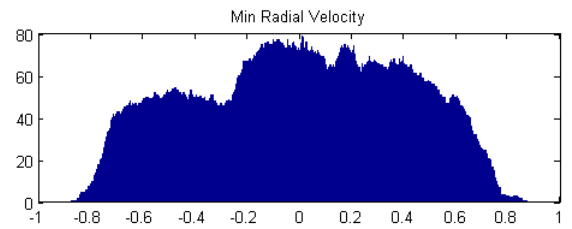
HD 99492 c



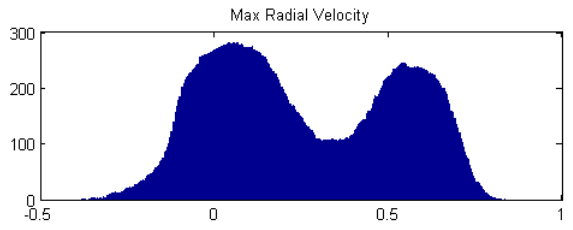
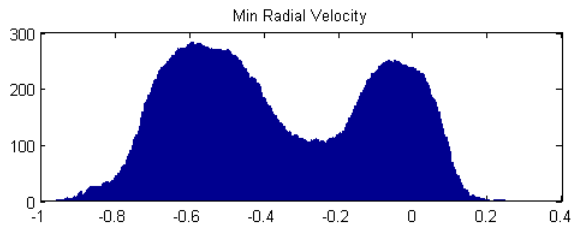
HD 217107 c



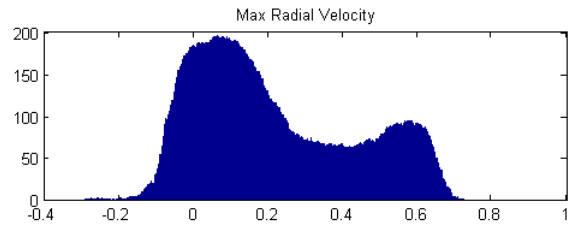
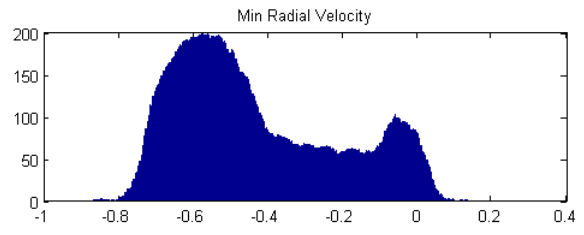
GJ 328 b



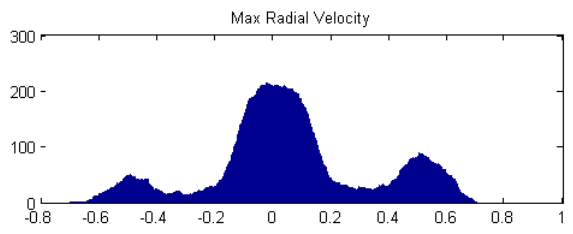
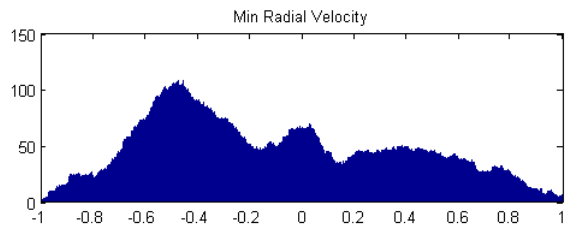
HD 142 c



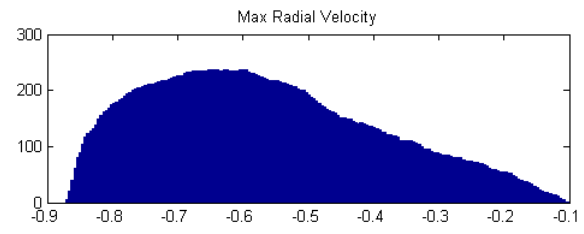
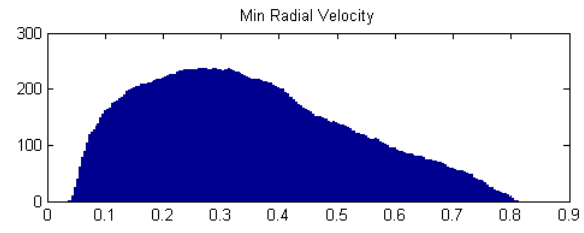
HD 114613 b



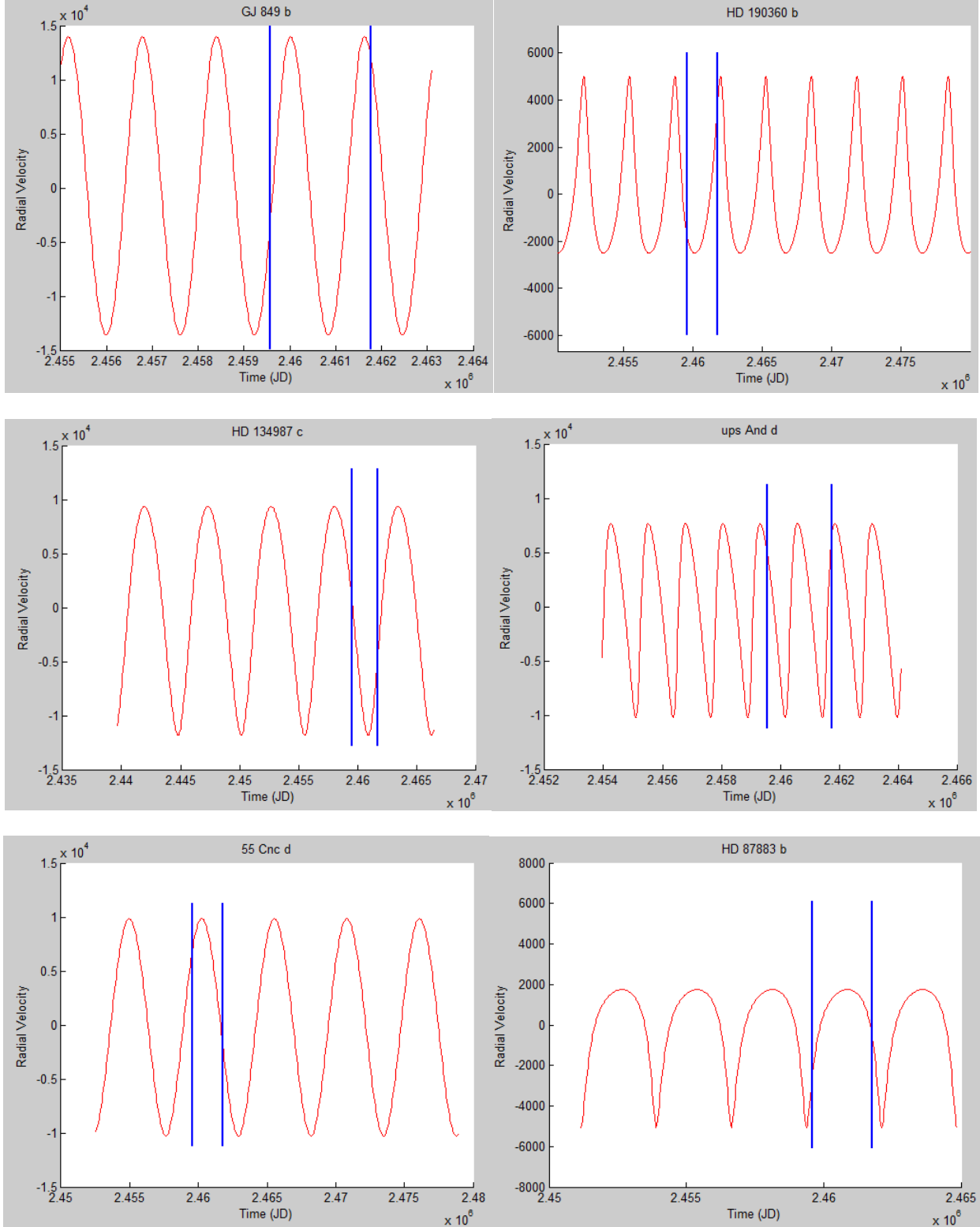
HD 134987 c

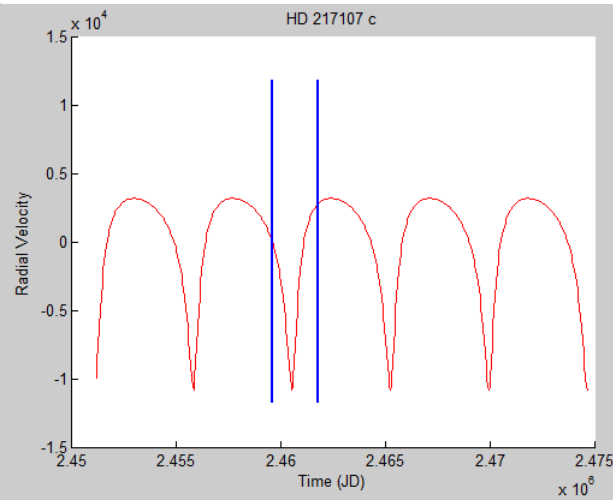
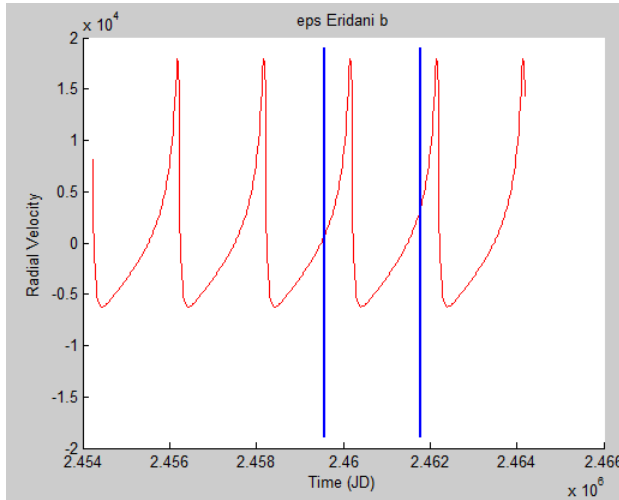
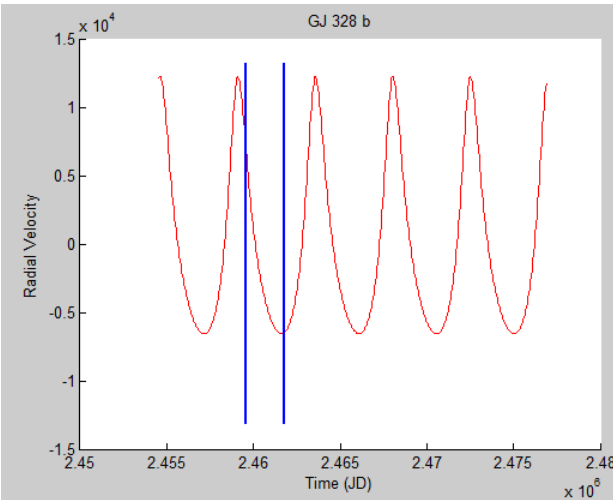
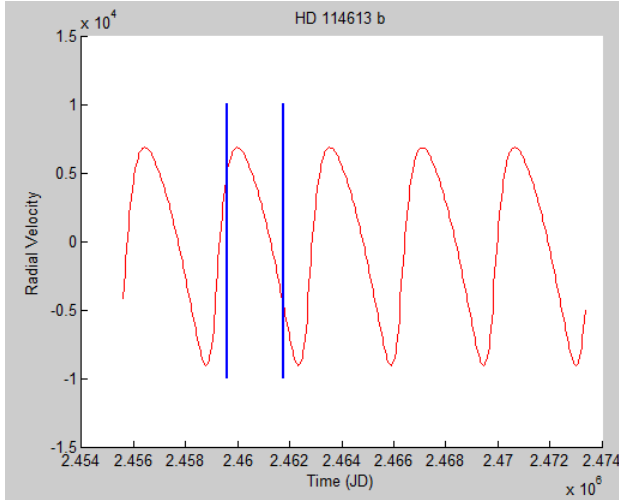
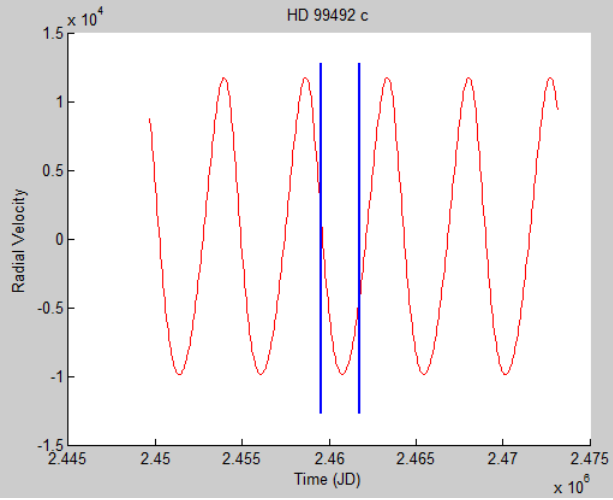
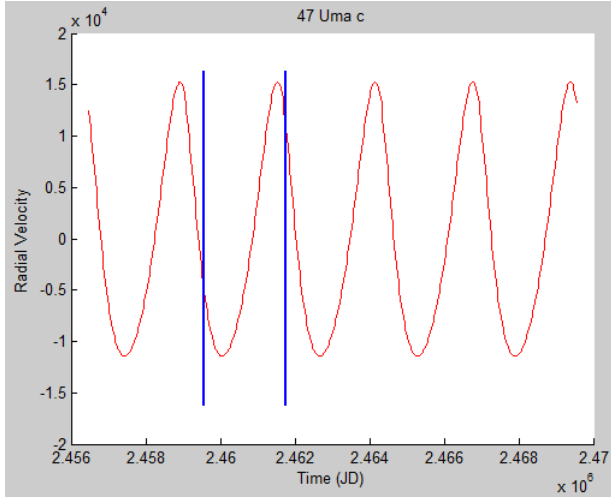


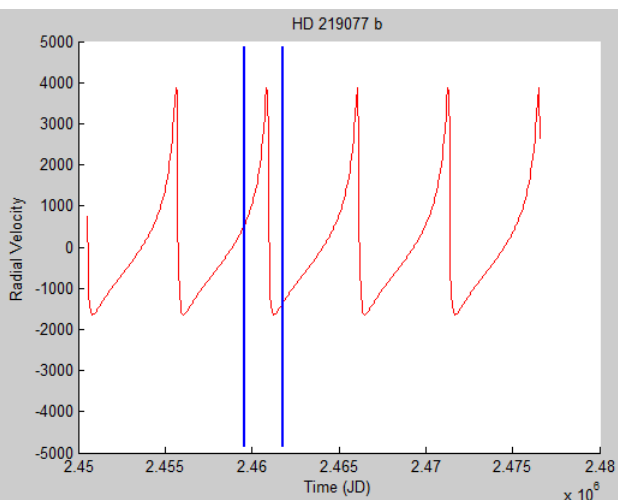
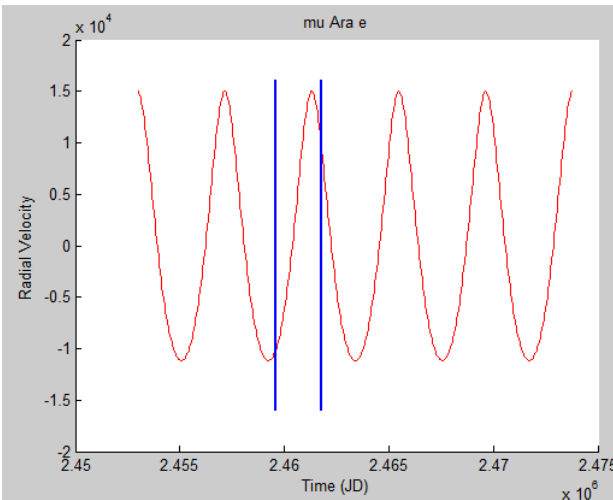
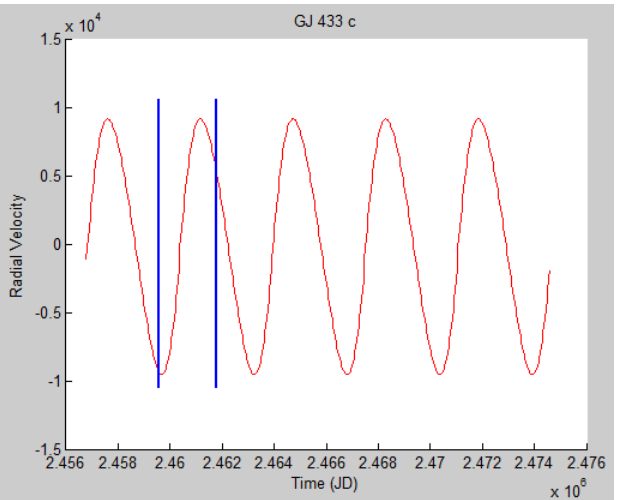
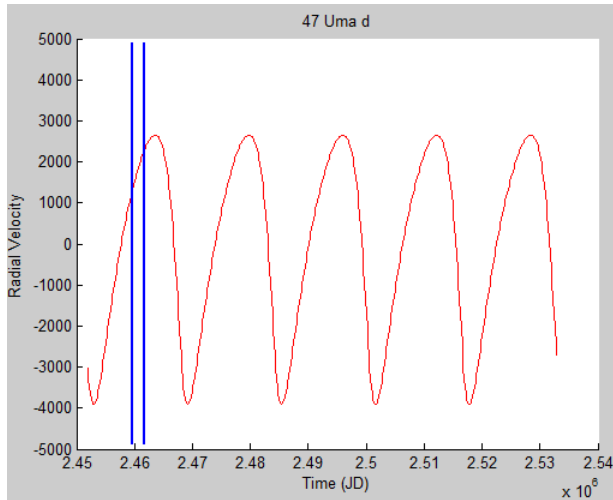
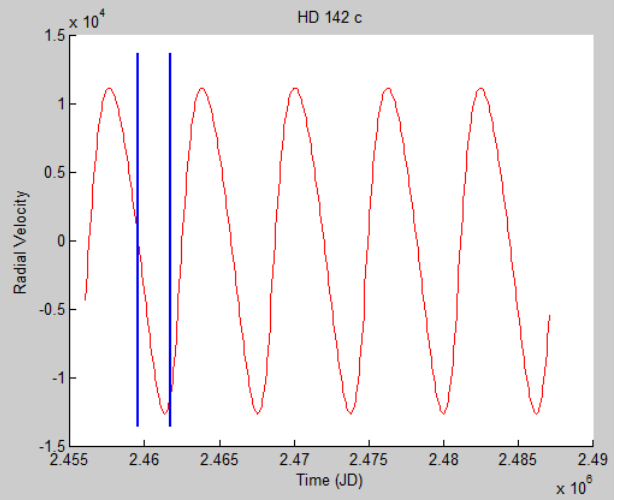
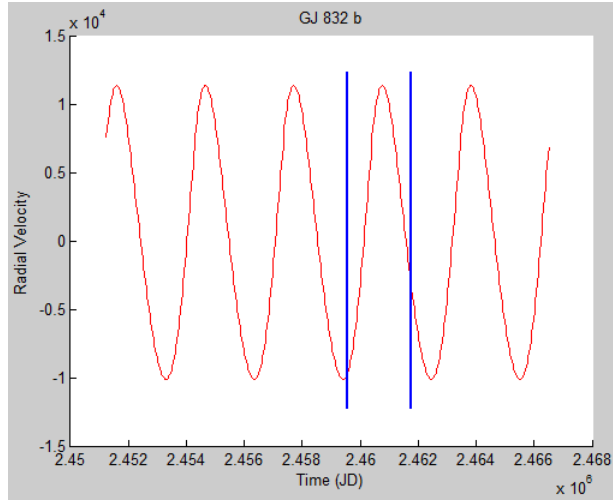
HD 219077 b

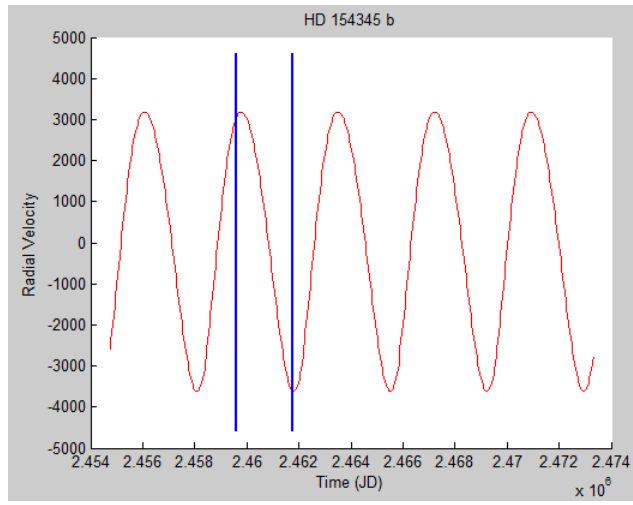


Appendix C – Radial velocity and time range profiles for each exoplanet

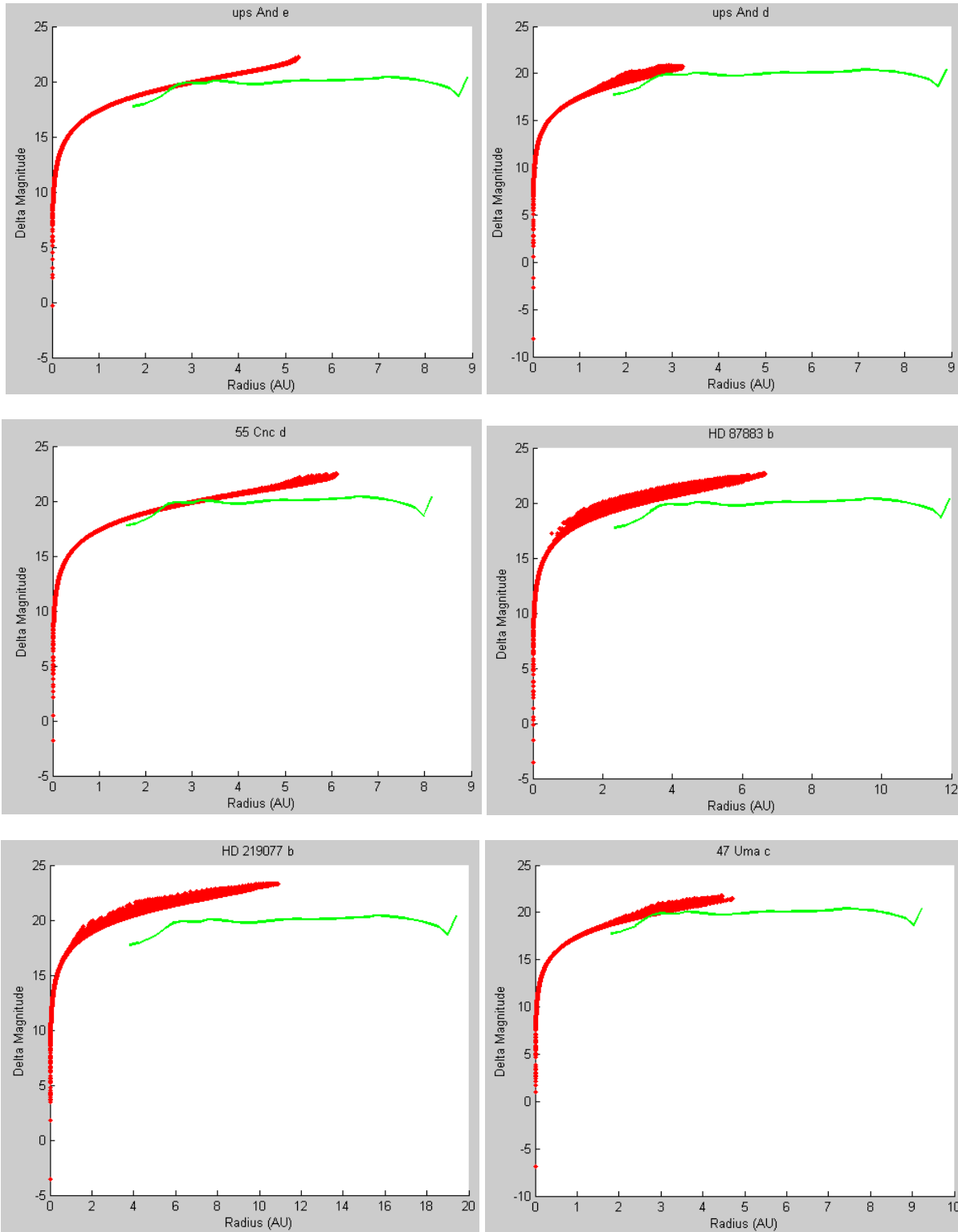


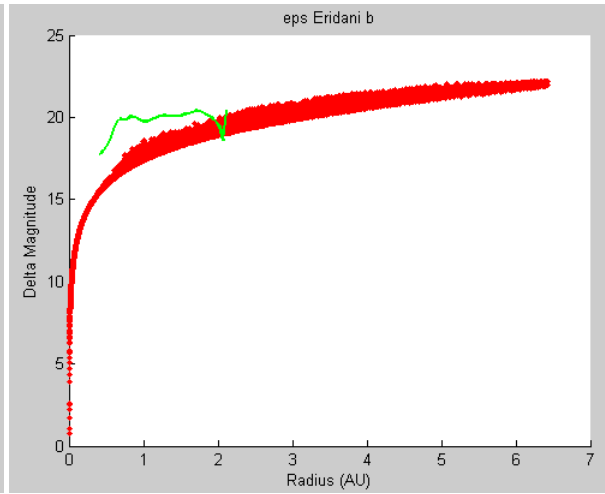
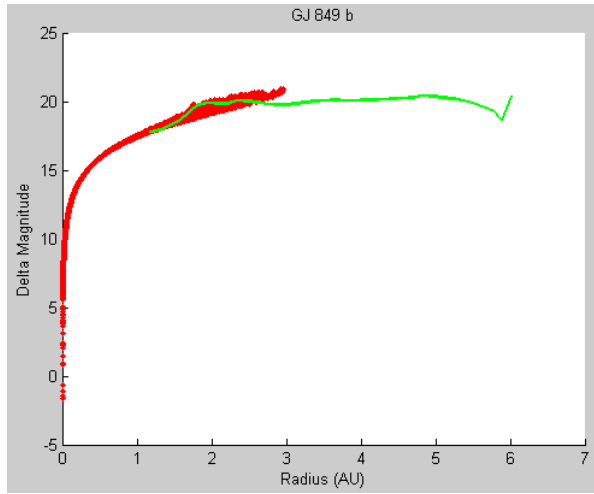
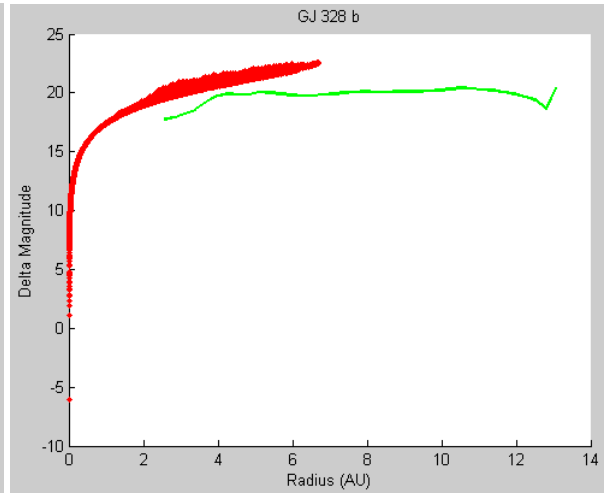
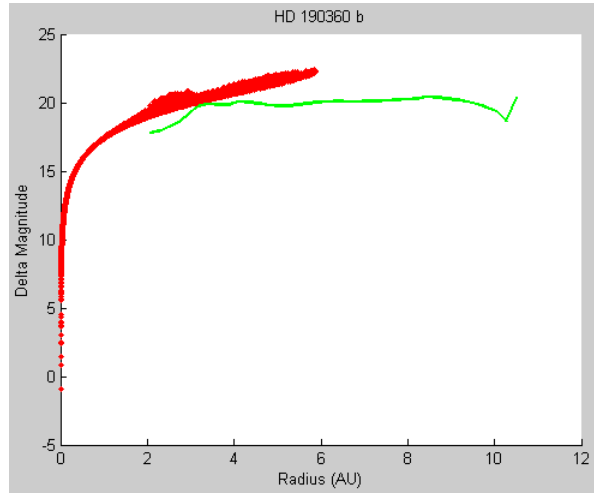
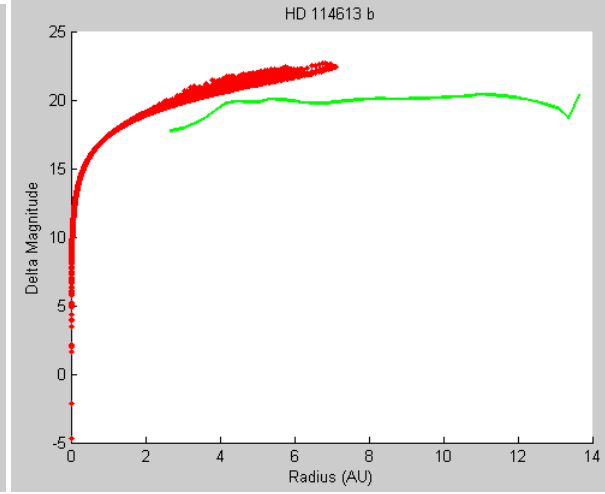
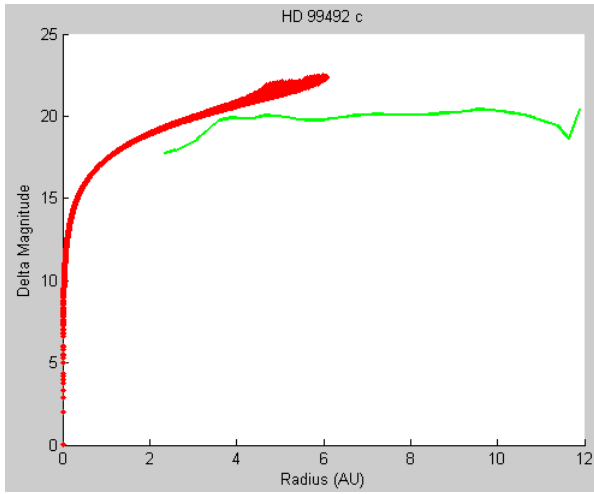


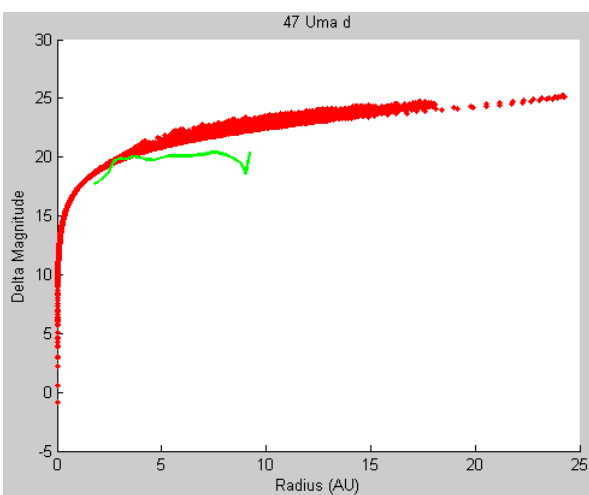
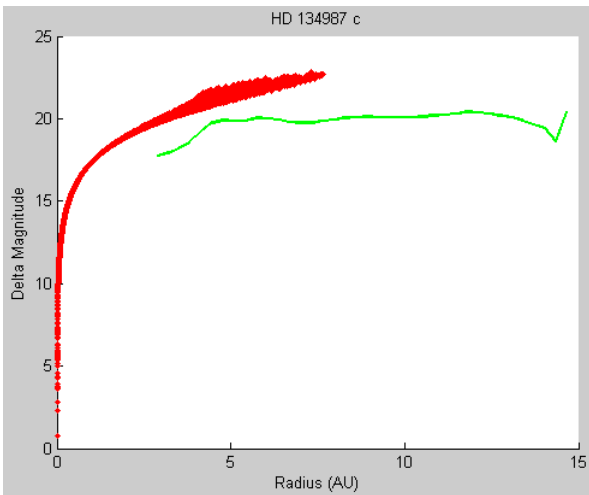
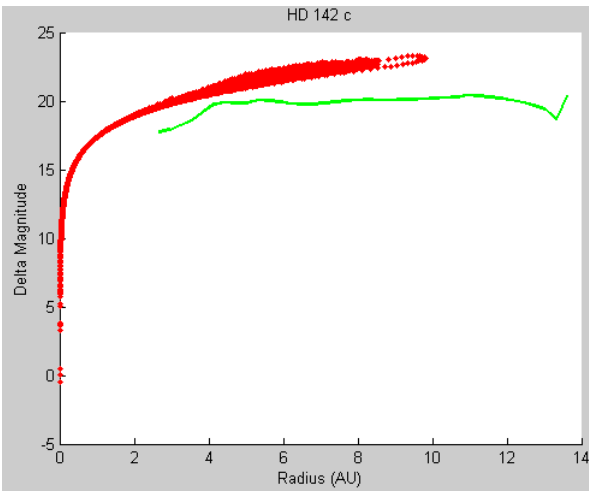
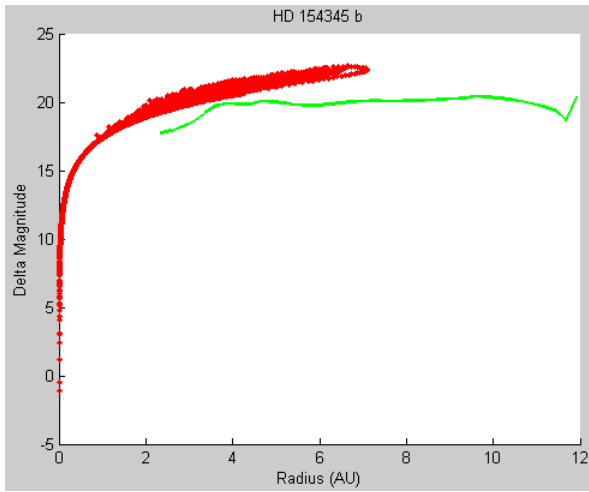
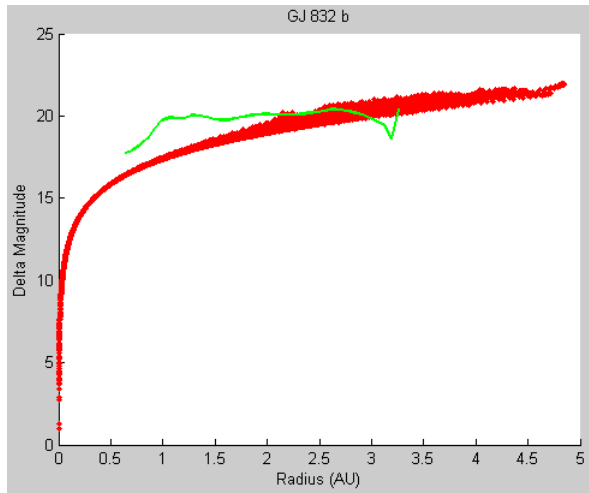
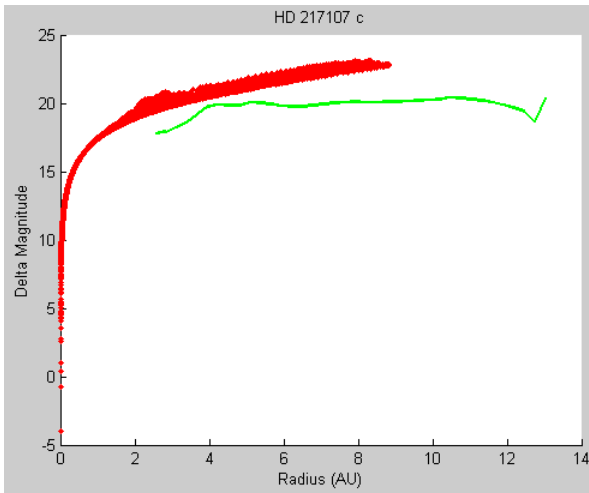


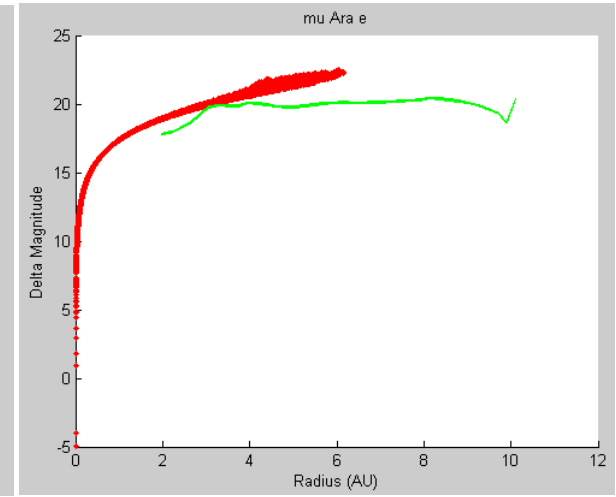
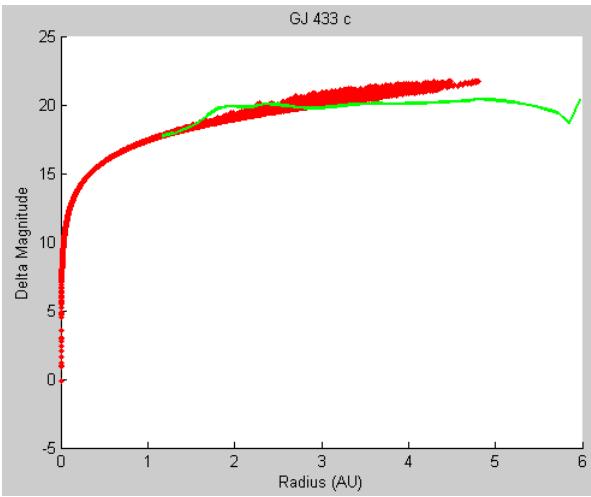
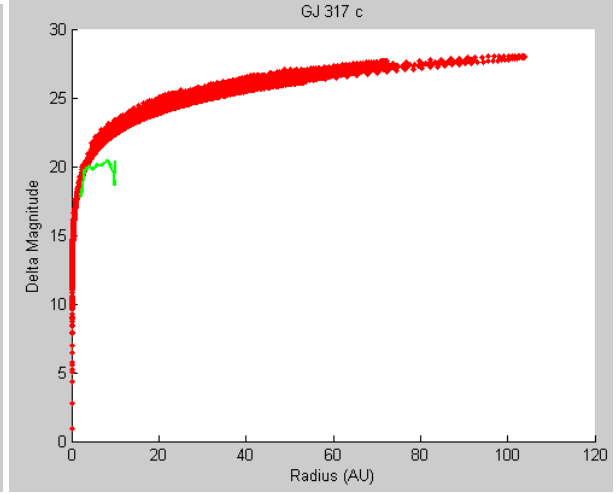
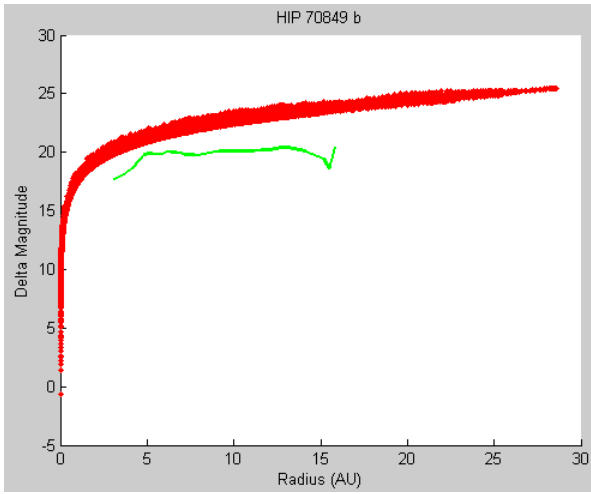


Appendix D – contrast curve limitations for each exoplanet









Appendix E – Main code used for orbital modeling and simulation

```
function [plname,time,radvel,dat,IWAr,timenormav,timevismin, ...
        timevismax,radius,totradius, Ds, Rpl] = exotimeall(pl);
% Number of orbits to simulate (num) and number of time intervals (int)
% num = 450; int = 250;
num = 200; int = 100;
% Set to 1 to show all figures, otherwise 0; set fn for fig num indexing
showallfigs = 0; fn = 1;
% Constant values
constant;

%% Extract necessary exoplanetary information from the Excel file
[dat,txt] = xlsread('exoplanetcatalog200iwa'); % Extracting data from
Excel
iwa = 200; % Inner working angle

%% Gathering all the planet information
for plno = pl % Change for multiple planets
plnum = plno; % Planet number - easily displayable
% Gathering all the necessary values for each planet
[plname, W, a, e, I, w, Mp, Ms, Ds, DSAU,Rpl] = planetinfo(plnum, dat, txt,
num);
disp('Planet:'); disp(plname); % Display planet name
% disp('Distance to star'); disp(DSAU); % Display our distance to the star

%% Calculation of needed values
mu = G*(Mp+Ms); % Gravitational parameter in (m^3/sec^2)
b = a.*sqrt(1-e.^2); % Semi minor axis in m
n = sqrt(mu./a.^3); % Mean motion
Tp = (2.*pi)./n; % Orbital period
Tp_av = mean(Tp)/daysTosec; % Mean orbital period
Tp_year = Tp_av/365.4;

%% Determination of eccentric anomaly, derivatives, and time using outside
function
[E, Edot, Eddot, time] = invKeplerVec(e,n,int);

%% Description of vectors A and B and obtaining radius and velocity
idx = 0;
for i = 1:num % For each orbit
A = a(i)*[-sin(W(i))*sin(w(i))*cos(I(i)) + cos(W(i))*cos(w(i)); ...
          sin(W(i))*cos(w(i)) + sin(w(i))*cos(I(i))*cos(W(i)); ...
          sin(I(i))*sin(w(i))];
B = b(i)*[-sin(W(i))*cos(I(i))*cos(w(i)) - sin(w(i))*cos(W(i)); ...
          -sin(W(i))*sin(w(i)) + cos(I(i))*cos(W(i))*cos(w(i)); ...
          sin(I(i))*cos(w(i))];
for j = 1:int
idx = idx+1;
rvec(idx,:) = A.*(cos(E(j,i))-e(i)) + B.*(sin(E(j,i)));
vvec(idx,:) = Edot(j,i).*(-A.*sin(E(j,i)) + B.*cos(E(j,i)));
radvel(j,i) = vvec(idx,3);
end
timenorm(:,i) = time(:,i)/time(int,i); % Normalize time by dividing each
% by the max time (at end of array)
end
```

```

% Conversions from vectors to matrices or vice versa
tvec = time(:); % matrix of time to a giant vector
tnormvec = timenorm(:); % normalized time from matrix to a vector
% Plot the 3D model and the radial velocity (if option to plot is selected)
if showallfigs == 1;
    % 3D model of all the orbits
    figure(fn); plot3(rvec(:,1),rvec(:,2),rvec(:,3),'.','MarkerSize',3);
    grid on; fn = fn+1;
    % Radial velocity
    figure(fn); plot(tvec(1:int),vvec(1:int,3)); ylabel('m/s');
xlabel('Days');
    fn = fn+1; figure(fn); plot(time(1:int),rvec(1:int,1)) % Sanity check
end

%% Implementation of the coronagraph specifications
% Values for IWA and OWA
IWA = iwa*mas; % Inner Working Angle in radians
OWA = 2*arcsec; % Outer Working Angle in radians
% Radius of IWA and OWA when projected on observer view
IWA_r = (IWA*Ds); % Radius of IWA in AU
OWA_r = (OWA*Ds); % Radius of OWA in AU
% Plotting the observer plane of observation
x0 = 0; y0 = 0; % Center of the circle for IWA and OWA
ang = linspace(0,2*pi,25); % Angles for plotting
x1 = IWA_r*cos(ang) + x0; % 'X' coordinate for the IWA circle
y1 = IWA_r*sin(ang) + y0; % 'Y' coordinate for the IWA circle
x2 = OWA_r*cos(ang) + x0; % 'X' coordinate for the OWA circle
y2 = OWA_r*sin(ang) + y0; % 'Y' coordinate for the OWA circle

% Plotting the viewable range and inner working angle blocked off area
if showallfigs == 1
    fn=fn+1; figure(fn); hold on; fill(x1,y1,'k');
    plot(rvec(:,1),rvec(:,2),'.','MarkerSize',3); hold off;
    fn=fn+1;
end

%% Determination of the times when the planet will be visible
% Radius when projected onto the 2D observer-view plane
for id = 1:num*int
    radius(id) = norm(rvec(id,1),rvec(id,2));
    totradius(id) = norm(rvec(id,:));
end
diff = radius' - IWA_r; % Difference of orbital radius - IWA
radius
idxvec = find(diff>0); % Indices for observable locations

%Using the index, finding the times when the planet is visible
for v = 1:length(idxvec)
    timeav(v) = tvec(idxvec(v));
    timenormav(v) = tnormvec(idxvec(v)); %Normalized
end
% Displaying histogram of all times
if showallfigs == 1;
figure(fn); hist(timenormav);
fn = fn+1;

```

```

end

%% Working with the radial velocity profile - min and max for each orbit
% Find the minimum and the maximum value for each orbit
rvmin = min(radvel); rvmax = max(radvel);
% Find the corresponding indices in the radvel matrix for the max and min
[minidx,minorb] = find(ismember(radvel,rvmin));
[maxidx,maxorb] = find(ismember(radvel,rvmax));
% Time for each orbit
for j = 1:num
    rvmintm(:,j) = timenorm(:,minorb(j)) - timenorm(minidx(j),minorb(j));
    rvmaxtm(:,j) = timenorm(:,maxorb(j)) - timenorm(maxidx(j),maxorb(j));
end
timemin = rvmintm(:); timemax = rvmaxtm(:);

%Only searching for the visible times
for v = 1:length(idxvec)
    timevismin(v) = timemin(idxvec(v));
    timevismax(v) = timemax(idxvec(v));
end
binsz = length(idxvec)/25; binsz = floor(binsz);

% Histogram of min and max radial velocity profiles
if showallfigs == 1;
    figure(fn);
    % subplot(3,1,1);
    plot(tvec(1:int)/daysTosec,vvec(1:int,3),'LineWidth',2); ylabel('m/s');
    xlabel('Days');
    % title(plname);
    subplot(2,1,1); hist(timevismin,binsz); title('Min Radial Velocity');
    subplot(2,1,2); hist(timevismax,binsz); title('Max Radial Velocity');
    fn = fn+1;
end
% Visibility percenter of the planet
VisPer = (length(idxvec)/length(tvec))*100;
end
end

```

Appendix F – Code used to gather all planetary information

```
function [plname, W, a, e, I, w, Mp, Ms, Ds, DSAU, Rplanet] =
planetinfo(plnum, dat, txt, num)
constant;
% Check to see eccentricity and semi-major axis are given
% Name of the planet
plname = txt(plnum+1,1);

% Mass of planet times sin(I) in kg
if isnan(dat(plnum,2)) % If no error bars
    Mpsi = dat(plnum,1)*Mjup;
else % If the error range exists
    Mpsi = dat(plnum,1)*Mjup + dat(plnum,2)*Mjup*randn(1);
end

% Longitude of ascending node
W = 2*pi*rand(num,1);

% Semi-major axis in meters
if isnan(dat(plnum,8)) % If no error bars
    a = dat(plnum,7)*AU*ones(num,1);
else % Normal distribution profile
    a = dat(plnum,7)*AU + dat(plnum,8)*AU*randn(num,1);
end

% Eccentricity
if isnan(dat(plnum,11)) % If no error bars
    e = dat(plnum,10)*ones(num,1);
else
    e = dat(plnum,10) + dat(plnum,11)*randn(num,1);
end % Normal distribution profile
for i = 1:length(e) % Making sure there aren't any negative eccentricities
    if e(i) < 0
        e(i) = 0;
    elseif e(i) >= 1;
        e(i) = .99;
    end
end
end
% e = zeros(num,1); % Test case

%Inclination in radians
if isnan(dat(plnum,13)) % If no data
    I = acos(2*rand(num,1)-1);
%    I = acos(rand(num,1))+(pi/4); % Edge-on case!
elseif isnan(dat(plnum,14)) % If no error bars
    I = dat(plnum,13)*degTorad*ones(num,1);
else % Normal distribution profile
    I = dat(plnum,13)*degTorad + dat(plnum,14)*degTorad*randn(num,1);
end

% Argument of periastron
if isnan(dat(plnum,16)) % If no data
    w = 2*pi*rand(num,1);
elseif isnan(dat(plnum,17)) % If no error bars
    w = dat(plnum,16)*degTorad*ones(num,1);
```

```
else % Normal distribution profile
    w = dat(plnum,16)*degTorad + dat(plnum,17)*degTorad*randn(num,1);
end
% w = zeros(num,1); % Test case

% Mass of planet in kg
Mp = Mpsi./sin(I);
% Mass of the star in kg
Ms = dat(plnum,24)*Msun;
% Distance to the star in m and AU
Ds = dat(plnum,23)*pcTom;
DSAU = dat(plnum,23)*pcToAU;
% Radius of the planet (size)
Rplanet = dat(plnum,25)*Rjup;
end
```

Appendix G – Supplementary subfunctions

```
function [Evec, Edotvec, Eddot, time] = invKeplerVec(e,n,int)
constant;
% M to represent the entire orbit
M = linspace(0,2*pi,int);
% Multiple iterations for each value of e
for i = 1:length(e)
    % Initial condition checking and setting
    E = M./(1-e(i));
    chck = E > sqrt(6*(1-e(i))./e(i));
    E(chck) = (6*M(chck)./e(i)).^(1/3);
    % Iteration process
    delta = 1;
    while abs(delta) > 10e-9
        f = M - E + e(i).*sin(E);
        fdel = e(i).*cos(E) - 1;
        E1 = E - f./fdel;
        delta = max(abs(E1 - E));
        E = E1;
    end
    % Setting the values
    Evec(:,i) = E;
    Edot = n(i)./(1-e(i).*cos(E));
    Edotvec(:,i) = Edot;
    Eddot(:,i) = -Edot.^2.*e(i).*sin(E)./(1-e(i).*cos(E));
    time(:,i) = (M./n(i))./daysTosec;
end
end
```

```
%% Constant values
G = 6.67384e-11; % Gravitational constant in m^3/(kg*s^2)
AU = 149597870700; % Astronomical unit in m
pcTom = 3.08567758e16; % Conversion from parsecs to meters
daysTosec = (24*3600); % Conversion from days to seconds
degTorad = (pi/180); % Conversion from degrees to radians
arcmin = (1/60)*degTorad; % Arcmin to radians
arcsec = (1/60)*arcmin; % Arcseconds to radians
mas = (1/1000)*arcsec; % Milli-arcsecond to radians
Mjup = 1.89813e27; % Mass of Jupiter in kg
Msun = 1.9891e30; % Mass of Sun in kg
pcToAU = 206264.806; % Conversion from parsec to AU
Rjup = 71492000; % Radius of Jupiter in meters
Rearth = 6378100; % Radius of Earth in meters
```

Appendix H - Code used for time range

```
function timerange(dateVec1,dateVec2,pl)
figno = 1;
showfigs = 1;
for id = 1:length(pl)
    % Start and end of the range of time we're looking at
    starttm = julianDate(dateVec1);
    endtm = julianDate(dateVec2);
    % Gather time and rv for the planet
    [plname,pltime,plrv,dat,IWArlim,tmnormav,tmvismin,tmvismax,radius,...
    totradius, Ds, Rpl] = exotimeall(pl(id));
    tperi = dat(pl(id),19);
    pltime = pltime(2:100,:); plrv = plrv(2:100,:); radius = radius'; radius
= radius(2:100);
    % Julian to calendar date
    [year,month,day,hour,minu,sec,dayweek,dategreg] = julian2greg(tperi);
    nwday = day + pltime; [m,n] = size(nwday);
    % Julian date for times
    for i = 1:m
        for j = 1:n
            jdtime(i,j) = julianDate([year month nwday(i,j) hour minu sec]);
        end
    end
    % Determine the period, and plot for a periodic time
    plper = jdtime(99,1) - jdtime(1,1);
    for k = 1:8
        pltm(((k-1)*99)+1:k*99,1) = jdtime(:,1) + (k-1)*plper;
        prv(((k-1)*99)+1:k*99,1) = plrv(:,1);
        plrad(((k-1)*99)+1:k*99,1) = radius(:,1);
    end
    pltm = sort(pltm);
    % Plotting
    if showfigs == 1
        figure(figno); hold all; plot(pltm,prv,'r');
        rn = ceil(max(abs(prv)))+1e3;
        line([starttm starttm],[-rn rn],'LineWidth',2);
        line([endtm endtm],[-rn rn],'LineWidth',2);
        title(char(plname)); xlabel('Time (JD)'); ylabel('Radial Velocity');
        figno = figno+1; figure(figno); hold all; plot(pltm,plrad,'g');
        plot(pltm,IWArlim,'LineWidth',2);
        rn = ceil(max(abs(plrad)))+1000;
        line([starttm starttm],[0 rn],'LineWidth',2);
        line([endtm endtm],[0 rn],'LineWidth',2);
        title(char(plname));
        xlabel('Time (JD)'); ylabel('Radius Viewable Range');
        figno = figno+1;
    end
end
end
end
```

Appendix I - Code used for contrast curve plotting

```
function contrastcurves(pl, fle)
constant;
showfigs = 1;
for id = 1:length(pl)
    % Gathering information from exotimeall
    [plname, time, radvel, dat, IWAR, timenormav, timevismin, timevismax, ...
        radius, totradius, Ds, Rpl] = exotimeall(pl(id));
    % Determing constrast information
    p = .5; % Given albedo for jupiter like planet at 550 nm
    beta = asin(radius./totradius); % Phase angle (star-planet-observer)
    Phi = (sin(beta) + (pi-beta).*cos(beta))./pi; % Lambert phase function
    delmag = -2.5.*log10(p.*Phi.*(Rpl./radius).^2); % Planet contrast
    % Obtaining the given constrast information
    %[datc,txtc] = xlsread('hlc_results2'); % Extracting data from Excel
    [datc,txtc] = xlsread(fle);
    contrast = datc(:,5); rad_as = datc(:,3); % Given contrast and radius
    radius_rad = rad_as*arcsec; % Radius in radian
    delmag0 = -2.5.*log10(contrast); % Delta magnitude of contrast
    radius_lim = radius_rad*Ds; % Limiting radius
    % Plotting the contrast curves and planet contrast info
    if showfigs == 1
        figure(pl(id)); hold on; title(char(plname));
        plot(radius/AU, delmag, 'r. ');
        plot(radius_lim/AU, delmag0, 'g', 'LineWidth', 2);
        xlabel('Radius (AU)'); ylabel('Delta Magnitude'); hold off
    end
end
end
```

Appendix J - Code used to plot overall time distributions

```
function allplanets(pl)
% Extract the information for each planet from exotimeall
% Used to create overall visibility profile
tvisallmin = []; tvisallmax = []; tvisallp = [];

for p = 1:length(pl)
    p
    [tvisall, tvismin, tvismax] = exotimeall(p);
    tvisallmin = [tvisallmin tvismin];
    tvisallmax = [tvisallmax tvismax];
    tvisallp = [tvisallp tvisall];
end
tvismin = tvisallmin(:); tvismax = tvisallmax(:); tvisall = tvisallp(:);
binz = length(tvisall)/100; binz = floor(binz);
figure(23); hist(tvismin,binz); title('Min Radial Velocity');
figure(24); hist(tvismax,binz); title('Max Radial Velocity');
figure(25); hist(tvisall,binz); title('Profile Over One Period');
max(tvismin);
end
```